UNITED REPUBLIC OF TANZANIA
Ministry of Energy
(MoE)
Dodoma

BUNDESREPUBLIK DEUTSCHLAND
Bundesanstalt für Geowissenschaften und Rohstoffe
(BGR)
Hannover

Promoting the Development of Geothermal Energy in Tanzania

Ground movements at Mt. Meru detected by InSAR

Dr. Kai Hahne

Hannover, December 2017

Ground movements at Mt. Meru detected by InSAR

Author	Dr. Kai Hahne (BGR)

Commissioned by	Federal Ministry for Economic Cooperation and Development (BMZ: Bundesministerium für wirtschaftliche Zusammenarbeit und Entwicklung)
Project Number	BMZ PN 2013.2250.2
BGR Number	05-2364
Implementing Agencies	Ministry of Energy of the United Republic of Tanzania (MoE) Tanzania Geothermal Development Company Limited (TGDC)
	Federal Institute for Geosciences and Natural Resources (BGR: Bundesanstalt für Geowissenschaften und Rohstoffe, Hannover)
Pages	58
Place and date of issuance	Hannover, December 2017

Table of Contents

Abbreviations

BGR	Bundesanstalt für Geowissenschaften und Rohstoffe (Federal Institute for Geosciences and Natural Resources)
DEM	Digital Elevation Model
DTM	Digital Terrain Model
GIS	Geographic Information System
GPS	Global Positioning System
InSAR	Interferometric Synthetic Aperture Radar (Spaceborne Radar Interferometry)
m asl	Metres above sea level
MoE	Ministry of Energy
OLI	Operational Land Imager (Sensor on board of Landsat 8 Satellite)
Pmax	Maximum principal stress
Pmin	Minimum principal stress
RADAR	Radio detection and ranging
RGB	Red Green Blue (colour band combination)
SBAS	Small base line subset. InSAR processing method
SRTM	Shuttle Radar Topography Mission
TGDC	Tanzanian Geothermal Development Company
TM	Thematic Mapper (Sensor on board of Landsat 5 Satellite)
TerraSAR-X (TSX)	German high resolution RADAR-Satellite
WP	Way Point (Measured by GPS)

List of figures

In figures, that show field photos, the location refers to a GPS waypoint (WP). All waypoints are listed in a table and a corresponding map in the appendix to allow traceability of the field survey.

Acknowledgement

My colleague **Ilona Grünberg** conducted the InSAR processing, which is fundamental for this report.

Although the available and usable data was close to the minimum required for analysis, she managed to get good and interpretable processing results using the method of Small Baseline Subset (SBAS).

Summary

A structural analysis based on multispectral satellite data and on high and medium resolution DEMs improves the geological and tectonic knowledge of a working area within the framework of a geothermal exploration programme in Northern Tanzania.

The mapped lineaments represent faults, strongly connected to the youngest movements of the ongoing rifting of the Neogene rifts.

Faults of WNW orientations dominate the Mt. Meru volcanic complex. Along these orientations, young hydrothermal alterations occur in the crater of the central ash cone as the youngest eruption centre.

The structural analysis is the basis for the interpretation of the SBAS based InSAR-processing results.

Southeast of Mount Meru, Linear zones of subsidence, with velocities of up to 136 mm per year occur. These zones follow the trends of existing lineaments, e.g. graben structures and aligned volcanoes.

Zones of high subsidence cover areas of moderate steepness as well as flat areas. Single zones extend over areas of different slope angles and different geological units. For this reasons, it is most likely, that neotectonic activity is the main factor for the development of these linear zones of subsidence.

By this time, available data, supporting geothermal exploration in a large scale is extremely limited. The area around Mt. Meru is hard to access due to steep terrain and thick vegetation cover. Considering the combined results from remote sensing studies, an area for further investigations can be suggested ESE of Mt. Meru for the following reasons:

- Occurrence of different lineament orientations, including the WNW orientation with young hydrothermal alterations in the central ash cone, and intersecting zones of high subsidence making this area highly permeable for any fluids.
- The flat to moderate topography in combination with an existing road offers good accessibility.

1 Scope of the Work

Within the bilateral project “Promoting the Development of Geothermal Energy in Tanzania” between BGR and the “Tanzanian Geothermal Development Company” (TGDC), the approach lies upon the estimation of the hydrothermal energy potential at Mount Meru.

Radar data cover huge areas and together with spaceborne Radar Interferometry (InSAR) processing, supplies an excellent method for the detection of ground movements in the range of a few millimetres per year.

In combination with structural analyses (see more details in report “Structural analysis of Mt. Meru and the surrounding area based on Remote Sensing data”), InSAR data can help to find locations of enhanced permeability for (hydrothermal) fluids and can also give hints for hydrothermal- and magmatic activities.

A first field-scoping mission in combination with a planning workshop in Arusha has been conducted together with partners of TGDC from 17/10/2016 to 26/10/2016. Findings of the field-scoping mission were presented at the workshop.

2 Working Area

The core working area for the geothermal exploration programme comprises Mt. Meru and its closest vicinity (Fig. 2.1, yellow frame, Fig. 2.2). InSAR analyses are focused on this core area, whereas the structural analyses (see more details in report *"Structural analysis of Mt. Meru and the surrounding area based on Remote Sensing data"*), which support the interpretation of InSAR results, incorporates the surrounding area with its variety of tectonic features (Fig. 2.1).

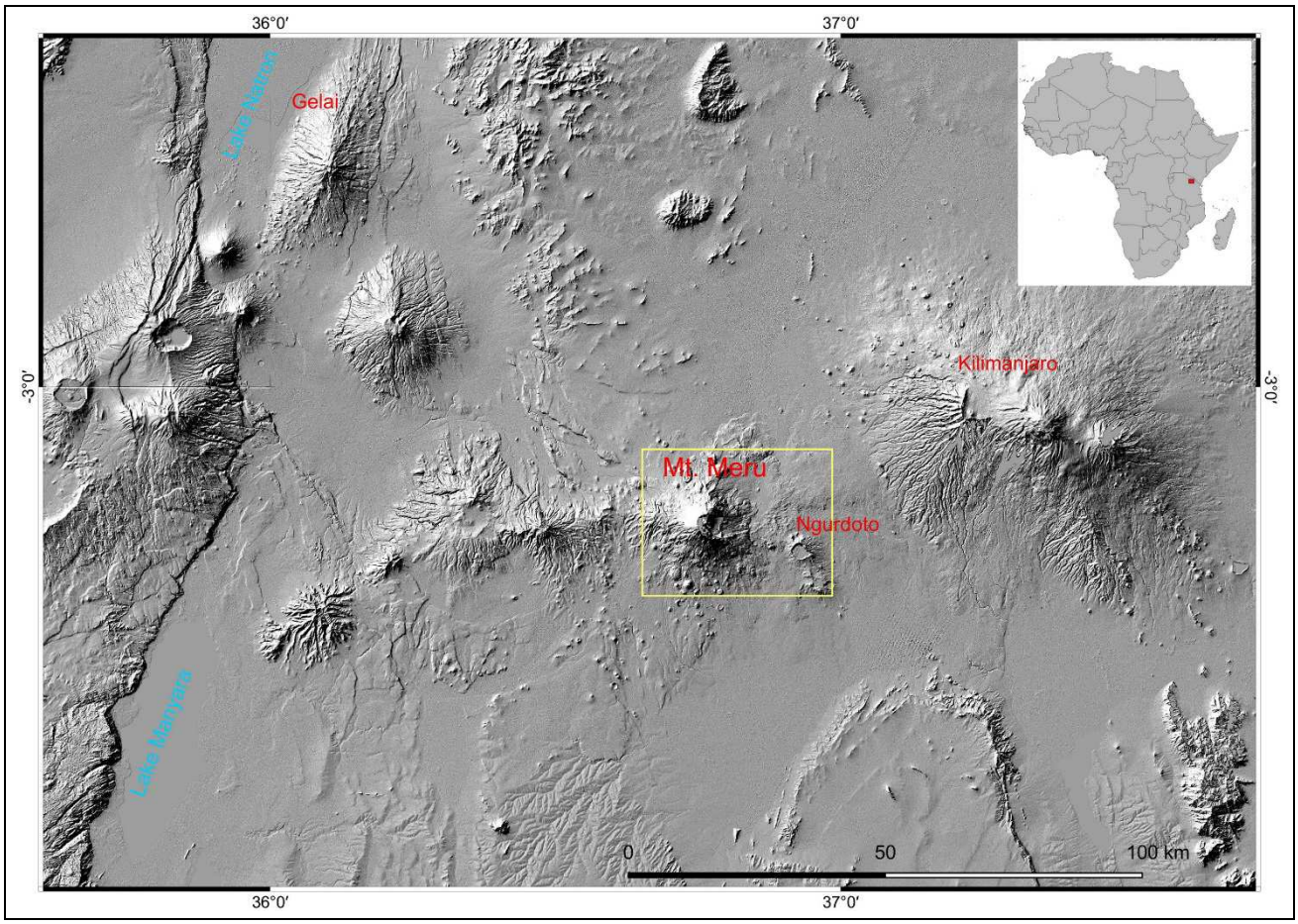

Figure 2.1: The major working area and the location of the core working area at Mount Meru (yellow frame) in Tanzania. 30 m SRTM elevation model shaded relief.

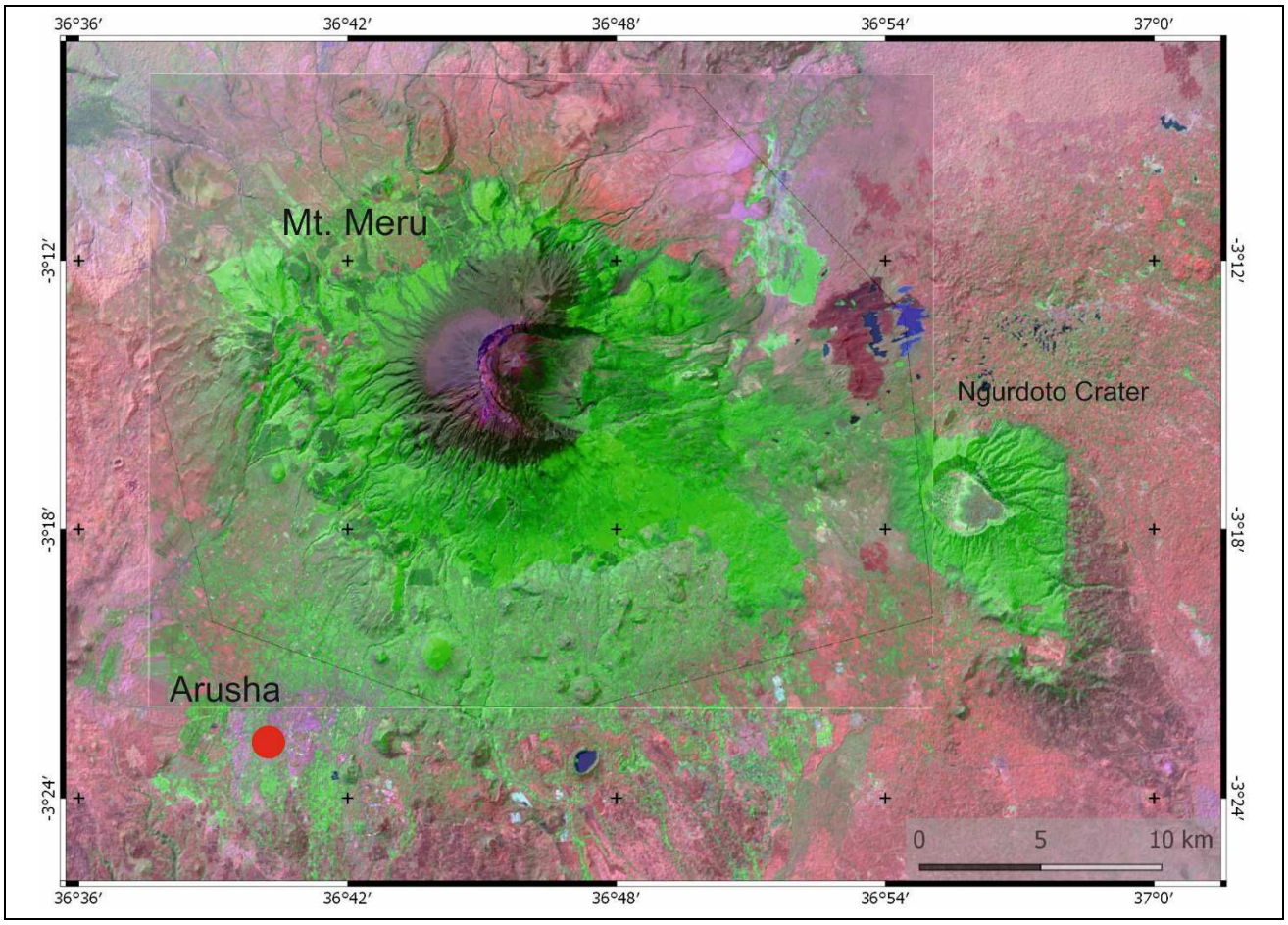

Figure 2.2: The working area with Mt. Meru. Landsat TM bands 7,4,1 (RGB). Projected onto high resolution 12m TerraSAR-X WorldDEM (Mt. Meru area only) and 30m SRTM DEM shaded relief.

3 Data

The following data are implemented in Quantum GIS (version 2.18.2) for further analysis and lineament vectorization:

- Enhanced and geocoded satellite images (using ENVI for e.g. highpass filtering, histogram stretching, shaded relief DEMs):
    - Landsat TM (30m ground resolution) acquired February, 02, 2000,
    - Landsat OLI (30m ground resolution) acquired January, 08, 2016,
    - Landsat OLI (30m ground resolution) acquired March, 10, 2016,
    - Landsat OLI (30m ground resolution) acquired August, 03, 2016,
    - SRTM 30m digital elevation model,
    - TerraSAR-X WorldDEM 12m digital elevation model.
- Vertical displacement maps as a result of InSAR processing from
    - RADARSAT-2, 24 scenes (10m ground resolution), processing period from 2013/07/28 to 2015/04/13.
- Geocoded raster data:
    - Geological map Arusha Quarter Degree Sheet 55 (WILKINSON, P. ET AL. 1983).
- Information from overview-field work (4 days only):
    - Shape and visibility of lineaments,
    - Additional geological and tectonic information,
    - Field photos,
    - Waypoints (WP) GPS measurements of findings and locations of photos.

The spatial reference system used for this study is UTM 37 S, WGS 84.

The following thematic layers have been created:

- Lineaments
- Normal Faults
- Normal Faults assumed

- Mt. Meru Slope Angles (0°-90°) based on TerraSAR-X WorldDEM
- Shaded relief maps from all available DEMs
- Waypoints with corresponding data tables concerning information from fieldwork (lithology, photos etc.).
- Displacement map
- Linear zones of subsidence.

Additional field photos- not mentioned in this report- and their locations, are attached on DVD to this report, designed as a Quantum GIS-project.

4 InSAR

Advanced interferometric SAR (Synthetic Aperture Radar) processing techniques are able to detect and monitor various surface displacements with mm accuracy.

A radar echo contains both amplitude and phase information. Most imaging radar applications use algorithms that utilize only the amplitude to extract physical surface characteristics. SAR interferometry exploits the phase difference between two radar echoes, associated with the same surface object, but measured by two different systems (or different times, respectively) along different directions. Measurement of such a phase difference is known as interferometry (Fig. 4.1). Radar Interferometry allows to measure surface elevation of individual image pixel, which leads to the generation of DEM's. The Radar phase of different images is sensitive to motion, (Fig. 4.1), which makes it possible to detect ground motion with an accuracy within millimetres per year via the radar´s phase shift. Therefore Radar interferometry is also used to measure surface motion, InSAR techniques either use a pair of images to generate short interval motion (e.g. earthquakes) or a set of data is collected to process motion in time (e.g. volcanic activities, mining, ground water exploitation) ULABY F.T.& LONG D.G., 2014.

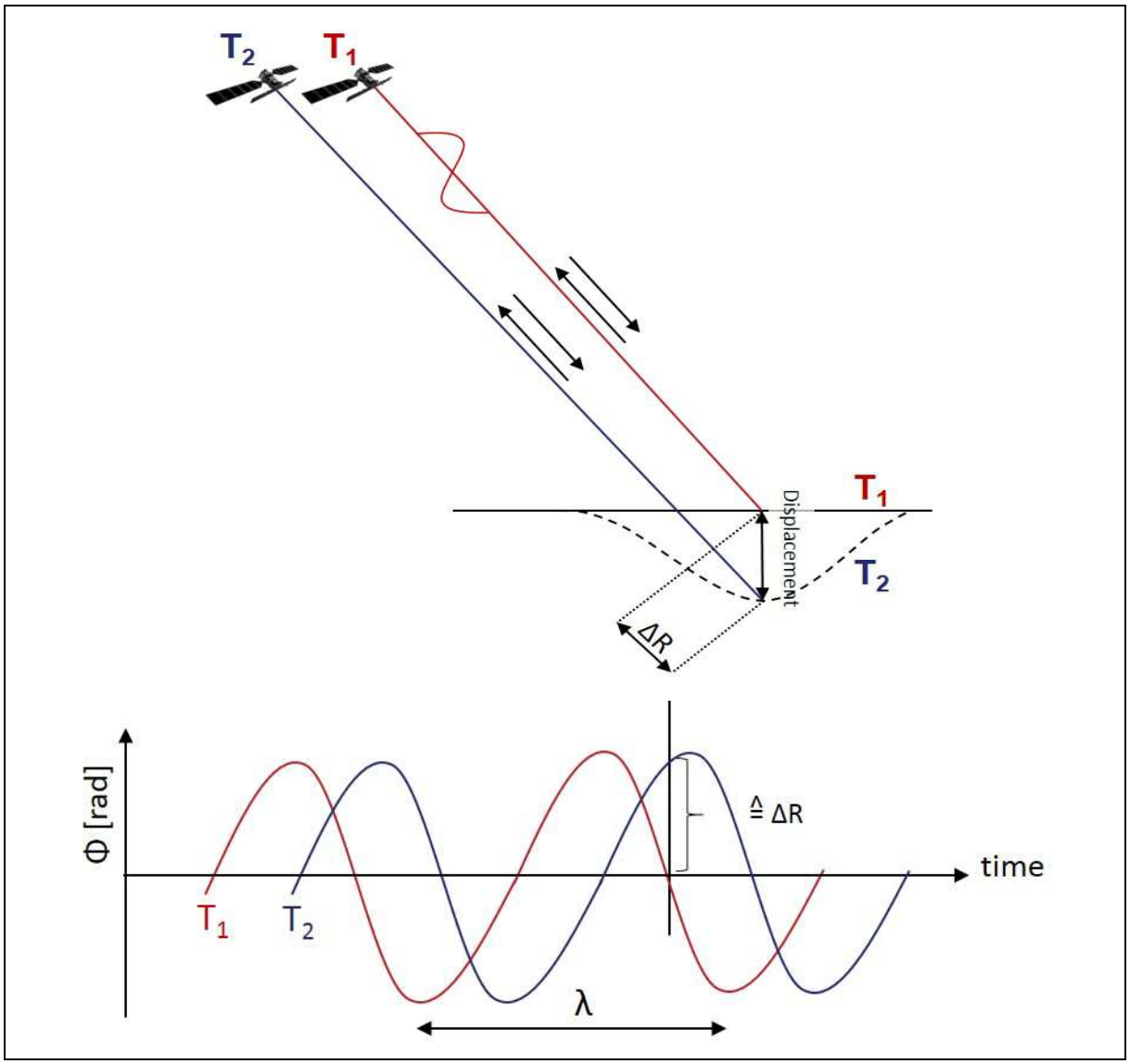

Figure 4.1: InSAR exploits the phase difference of at least two SAR images to detect vertical ground movement. T_1 = time of acquisition for the first image, T_2 = acquisition time for the second image, λ = wavelength, ΔR = range difference distance.

For our study at Mount Meru, the most suitable algorithm for InSAR processing was the Small Baseline Subset (SBAS, BERARDINO ET AL. 2002), as this method delivers also reliable results in vegetated areas, where others would fail due to lacking scatterers (e.g. persistent scatterer interferometry, PSI).

The method is based on the combination of differential interferograms and allows the computation of a time series of the deformation and is especially suitable for vegetated areas. The SBAS method allows a time series analysis to detect non-linear surface deformations.

We used 24 RADARSAT-2 scenes of the ascending path in “wide fine” beam mode and horizontal-horizontal (HH) polarisation (RADARSAT-2, 2016). The resulting ground resolution is 10 metres. The maximum small baseline is 96 days and the entire scene size of 176 km X 176 km is processed to get sufficient stable reference points. Stable areas are characterised by relatively high coherence

(in our case better than 0.25) and are mainly located in topographically flat parts of the scenes. In those areas, assumed to be stable, ground control points are set manually. All observed ground motions are relative to these stable points.

The resulting velocity maps are described and interpreted in chapter 7.

5 Geology

The core working area around Mount Meru is situated in the Northern Tanzanian Divergence Zone (Fig. 5.1) and is built up of Precambrian rocks of the Tanzania Craton (Archaean) and the north-south trending Mozambique orogenic fold belt (Archean/Proterozoic, BEECKMANS, B., (2014), DAWSON (2008), Fig. 5.1). The Tanzania Craton has an elevation above 1100 m. This supports the existence of a subcratonic plume whose evidents can be seen in the volcanics at both branches of the rift system (BEECKMANS, B., 2014).

Mount Meru – a 4565m high stratovolcano – and its surrounding area is built up of multi-phase volcanic products as flood basalts - which represent the oldest products - lavas, pyroclastics and lahars (Figures 5.2, 5.3), which were reinterpreted as debris avalanches by DELCAMP ET. AL. (2016). All these volcanites overlie the Precambrian basement.

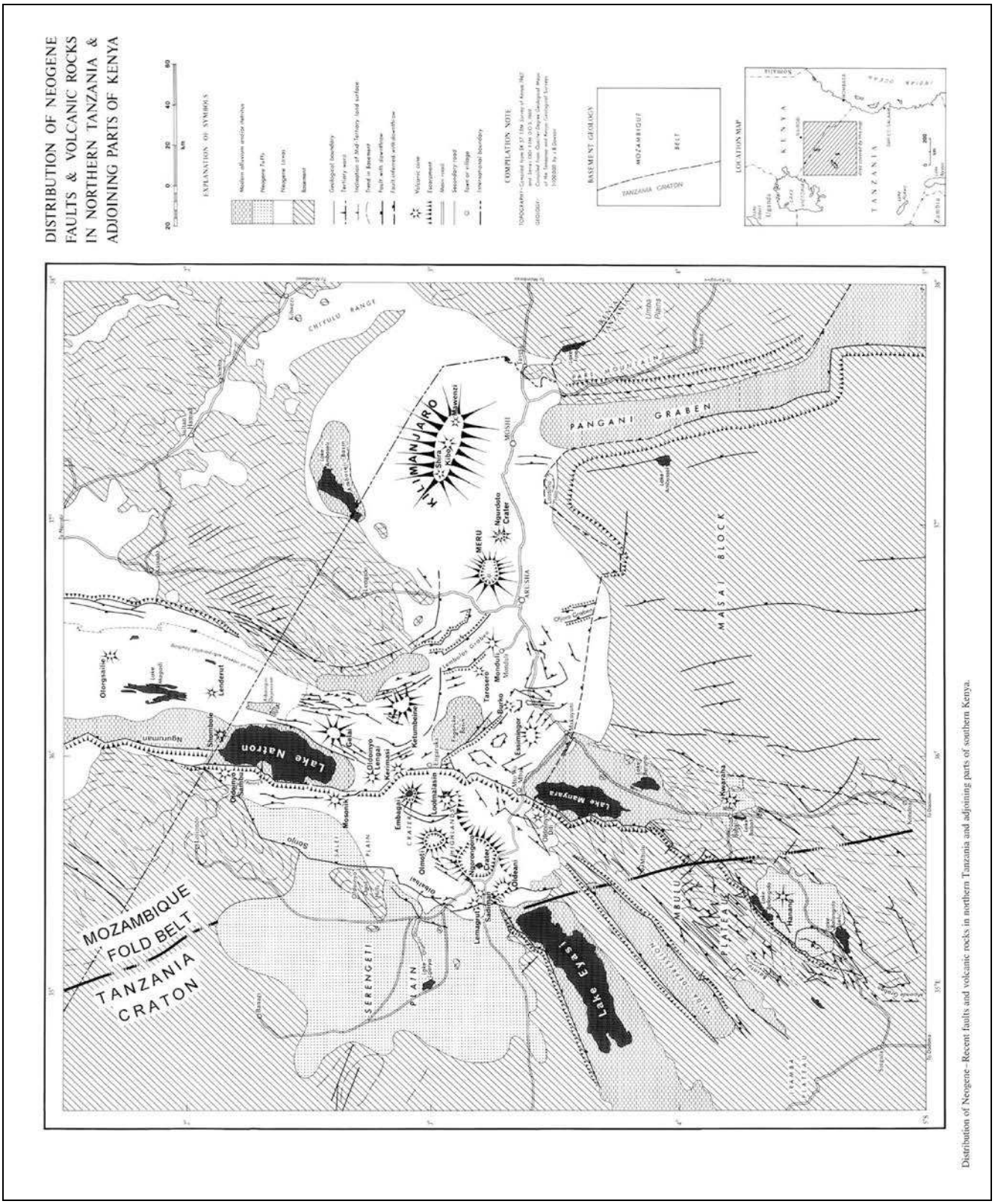

Figure 5.1: The Northern Tanzanian Divergence Zone, DAWSON (2008).

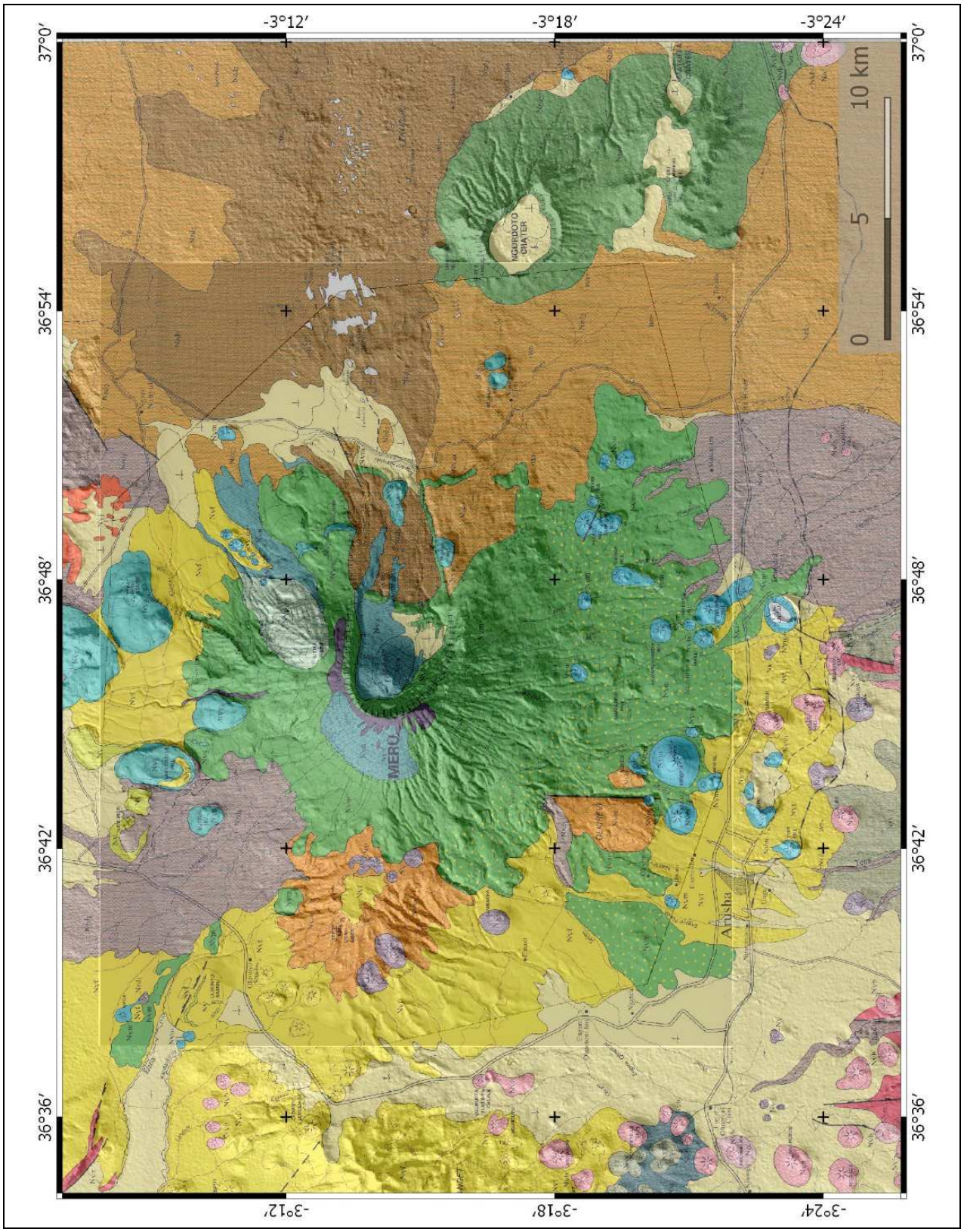

Figure 5.2: The Geology of Mt. Meru area after WILKINSON, P. ET AL (1983) projected onto TSX WorldDEM and SRTM DEM, shaded relief. Legend see figure 5.3.

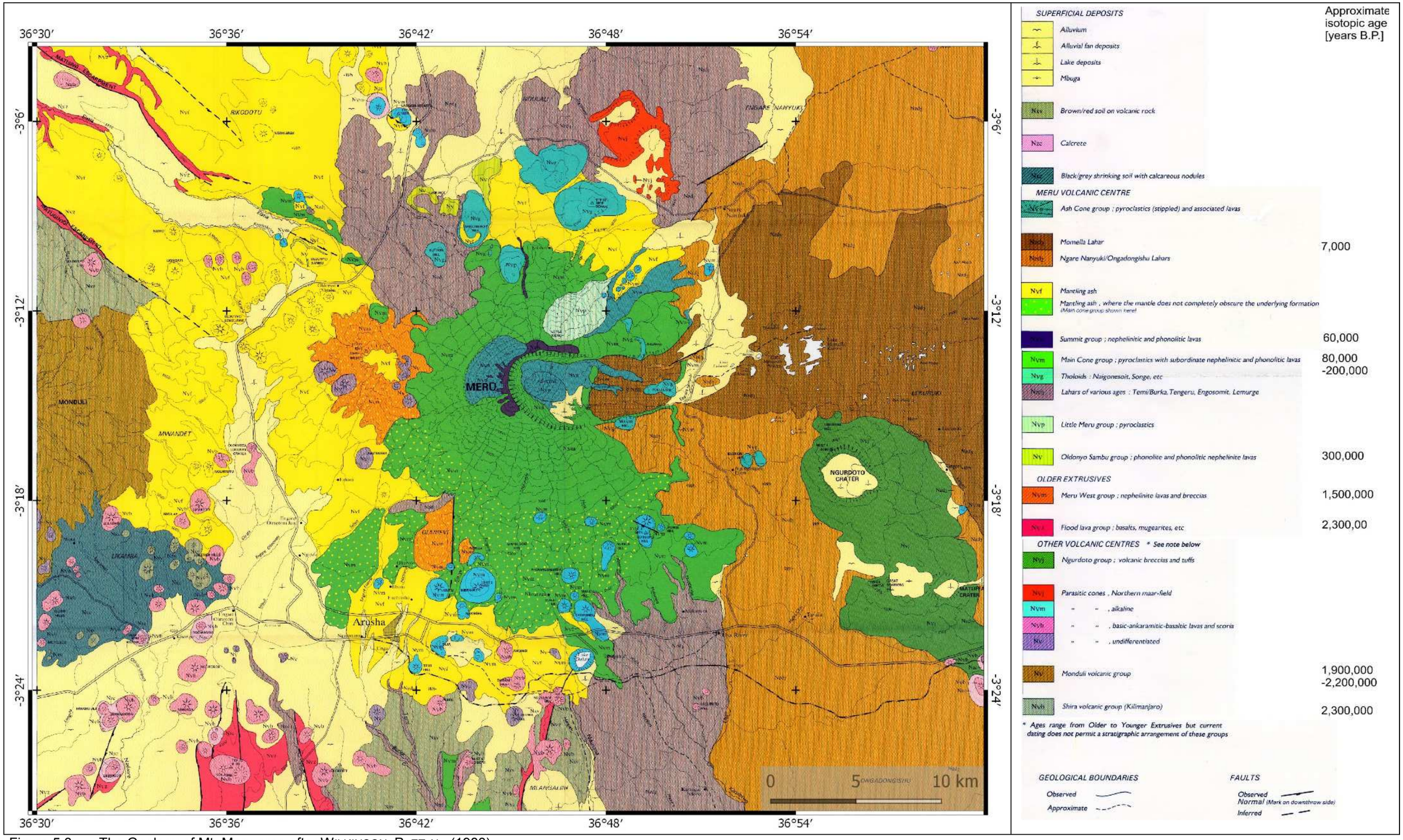

Figure 5.3: The Geology of Mt. Meru area after WILKINSON, P. ET AL. (1983).

A striking feature of Mt. Meru is the missing eastern flank (Fig. 5.4). This typical horseshoe-shaped scar formed after a sector collapse of Mt. Meru approximately 8600 years B.P. (SIEBERT, L., 1984) respectively 7000 years B.P. (after WILKINSON, P. ET AL., 1983), depositing huge debris avalanches (DELCAMP ET. AL., 2016) (described as "lahars" by WILKINSON, P. ET AL., 1983). These debris avalanches reach out to the east to the lower slopes of Mt. Kilimanjaro and cover approximately 1500 km^2 (WILKINSON, P. ET AL., 1983). ROBERTS (2002) calculated the volume of the debris avalanches to 28 km^3 by modelling the pre-collapse surface of Mt. Meru.

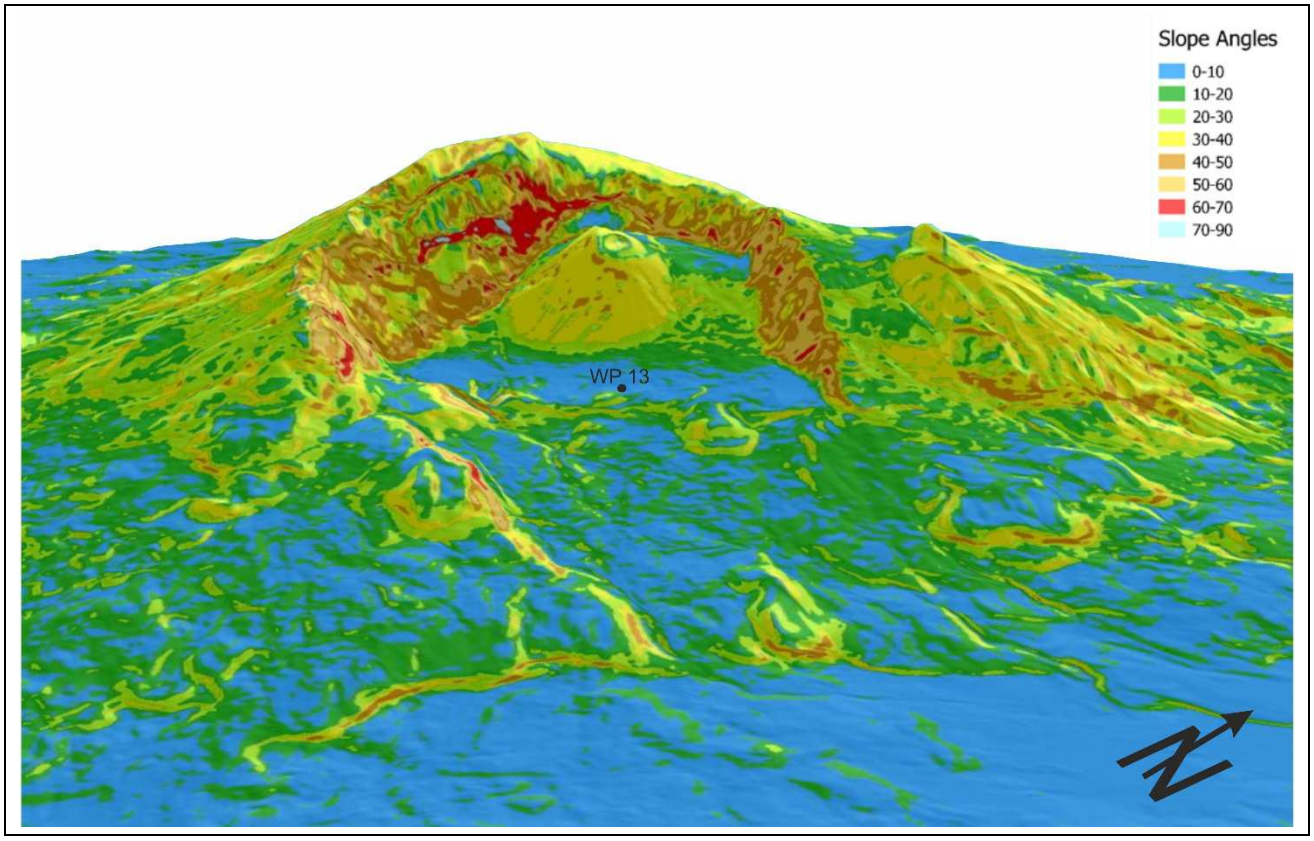

Figure 5.4: The collapsed eastern flank of Mt. Meru. Slope angle map derived from TSX WorldDEM projected over TSX DTM shaded relief. Perspective view into the crater with the central ash cone. 1.5 X vertical exaggeration.

Mt. Meru is an active volcano, which last erupted black ash from the central ash cone (Figures 5.4, and 5.5) in 1910, furthermore, significant fumarolic activity was recorded 1954 in the central ash cone (Fig. 5.6) and might have ceased before 1974 (WILKINSON, P. ET AL., 1983). Warm, mineralised springs (23°C) are present especially in the eastern crater area.

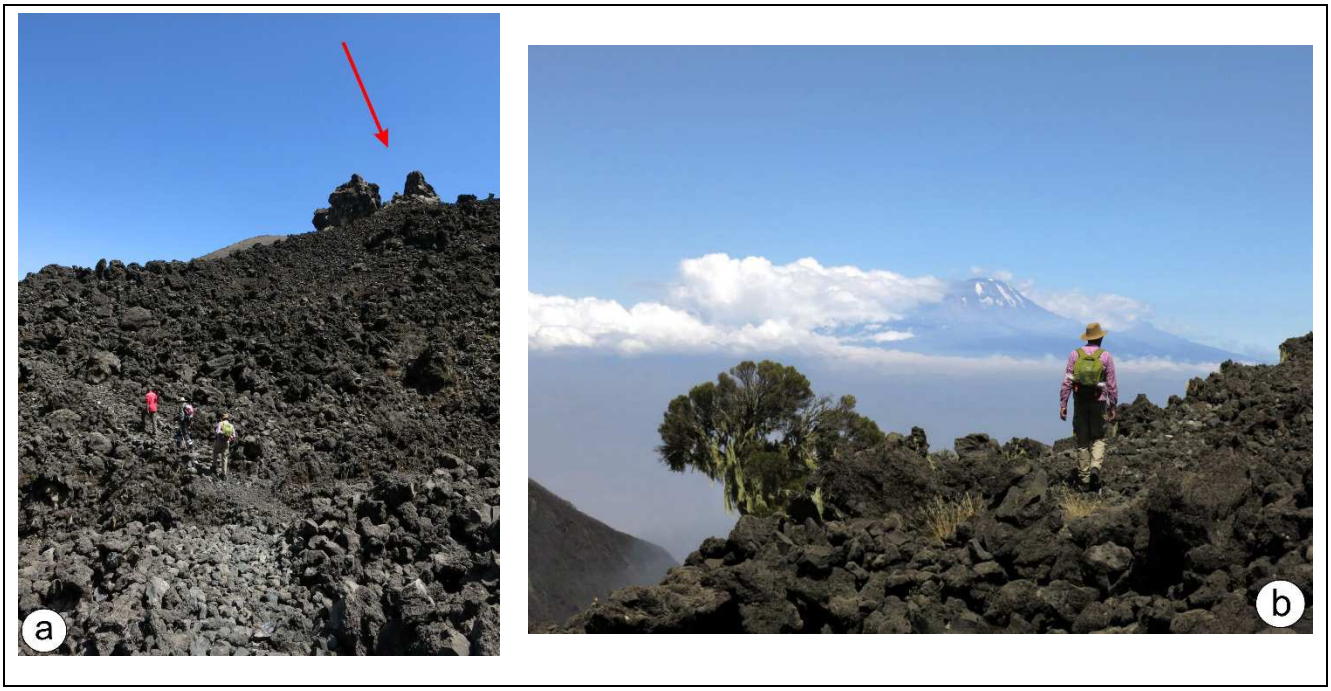

Figure 5.5: a: Youngest lavas of the Ash Cone Group with lava dome (red arrow), view to the south, WP9. b: Youngest lavas of the Ash Cone Group. View to the east with Mt. Kilimanjaro in the background.

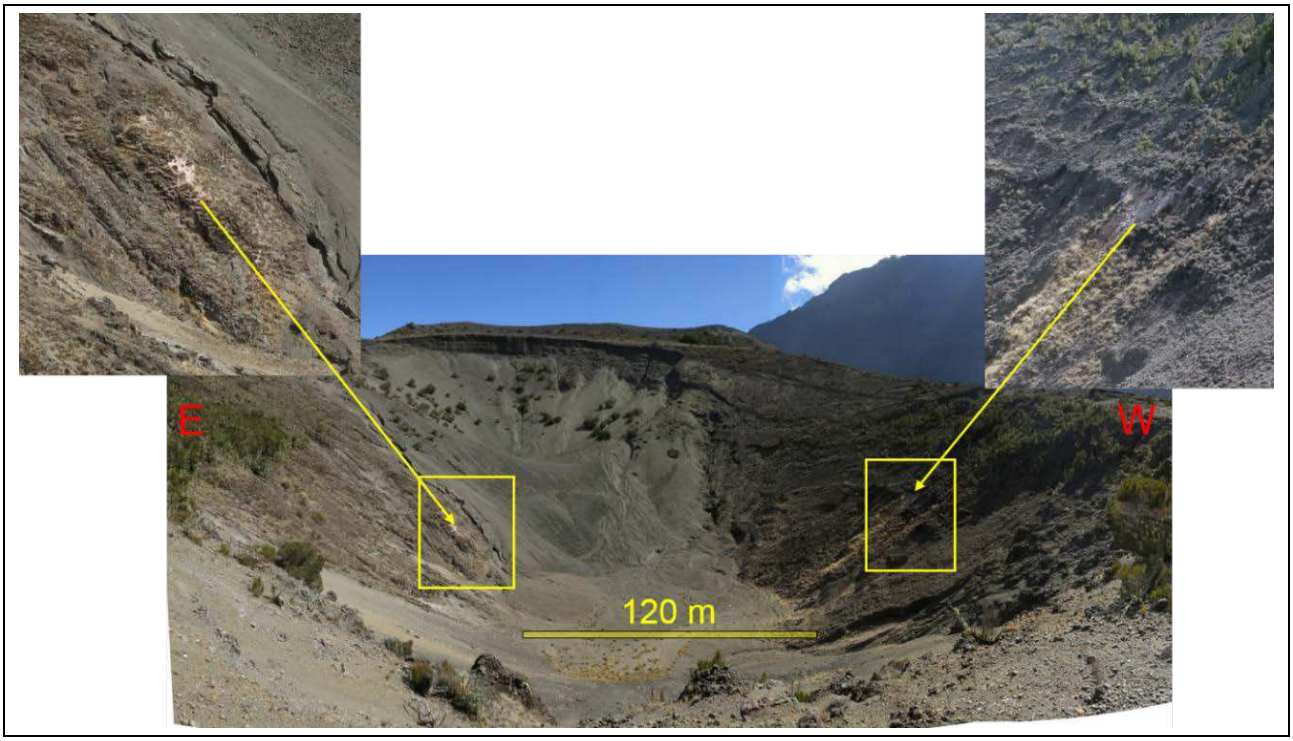

Figure 5.6: Hydrothermal alterations at the inner east and west flanks of the central ash cone´s crater. View to the south, WP11.

6 Tectonic setting

Three distinct rifts with different orientations (FOSTER ET AL., 1997) dominate the working area in the Northern Tanzanian Divergence Zone:

1. The Natron-Manyara-Balangida Rift (N-S-trending),
2. the Eyasi-Wembere Rift (NE-trending) and
3. the Pangani Rift (NW-trending).

The rifts are named after the lakes, which have developed on the rift bottoms. They transect the lithospheric boundary between the Archean (Tanzania Craton) and the Proterozoic (Mozambique orogenic fold belt), (Figure 5.1). An example of tectonics of Archean rocks is shown in figure 6.1, where multiphase folding is observed (orange lines). The NW trending Pangani Graben is built up by rocks of the Proterozoic Mozambique orogenic fold belt.

The orientations of the major rifts and the orientations of aligned volcano-chains (Fig. 6.1), are variable and display the changing tectonomagmatic conditions and are a result of the interplay between:

- The regional stress field,
- the local magma-induced stress field and
- stress rotations by mechanical interaction of rift segments (MUIRHEAD ET. AL., 2015).

The magma intrusion forming aligned volcanic-chains (Figure 6.1) widely follows Precambrian basement structures and (reactivated) faults.

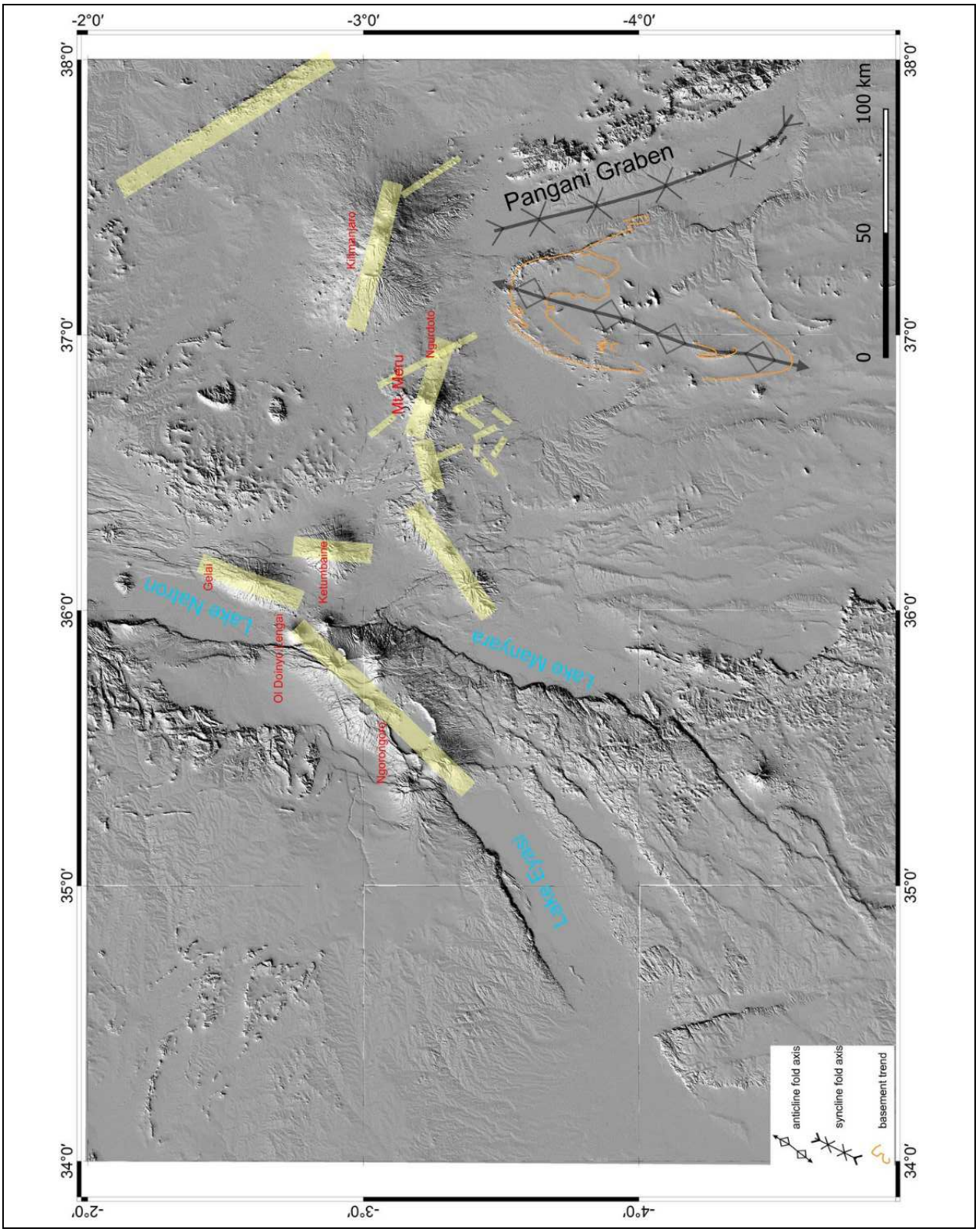

Figure 6.1: Northern Tanzanian Divergence Zone with Natron-Manyara-, Eyasi- and Pangani rifts (named after the lakes often developed on the rift bottoms) with different orientations. The variable orientations of aligned volcano-chains (yellow stripes showing examples) display the changing tectonomagmatic conditions. The intrusion widely follows Precambrian basement structures and (reactivated) faults. One example for Archean basement structures, which shows multiphase folding is highlighted by orange lines. The NW trending Pangani Graben is built up by rocks of the Proterozoic Mozambique orogenic fold belt. Shaded relief SRTM DEM mosaic.

6.1 Lineaments

The majority of the mapped lineaments represents faults (Fig. 6.2). Wherever possible, “normal faults” were distinguished from other “lineaments”. The faults are strongly connected to the ongoing rifting of the Neogene rifts. Normal faults impressively offset older shield volcanoes as Gelai and Ketumbaine (Fig. 6.3). This faulting follows a NE direction at Gelai and turns to a NW direction slightly farther south at Ketumbaine, displaying the change of the structural trends of the Precambrian basement (see also Figure 5.1).

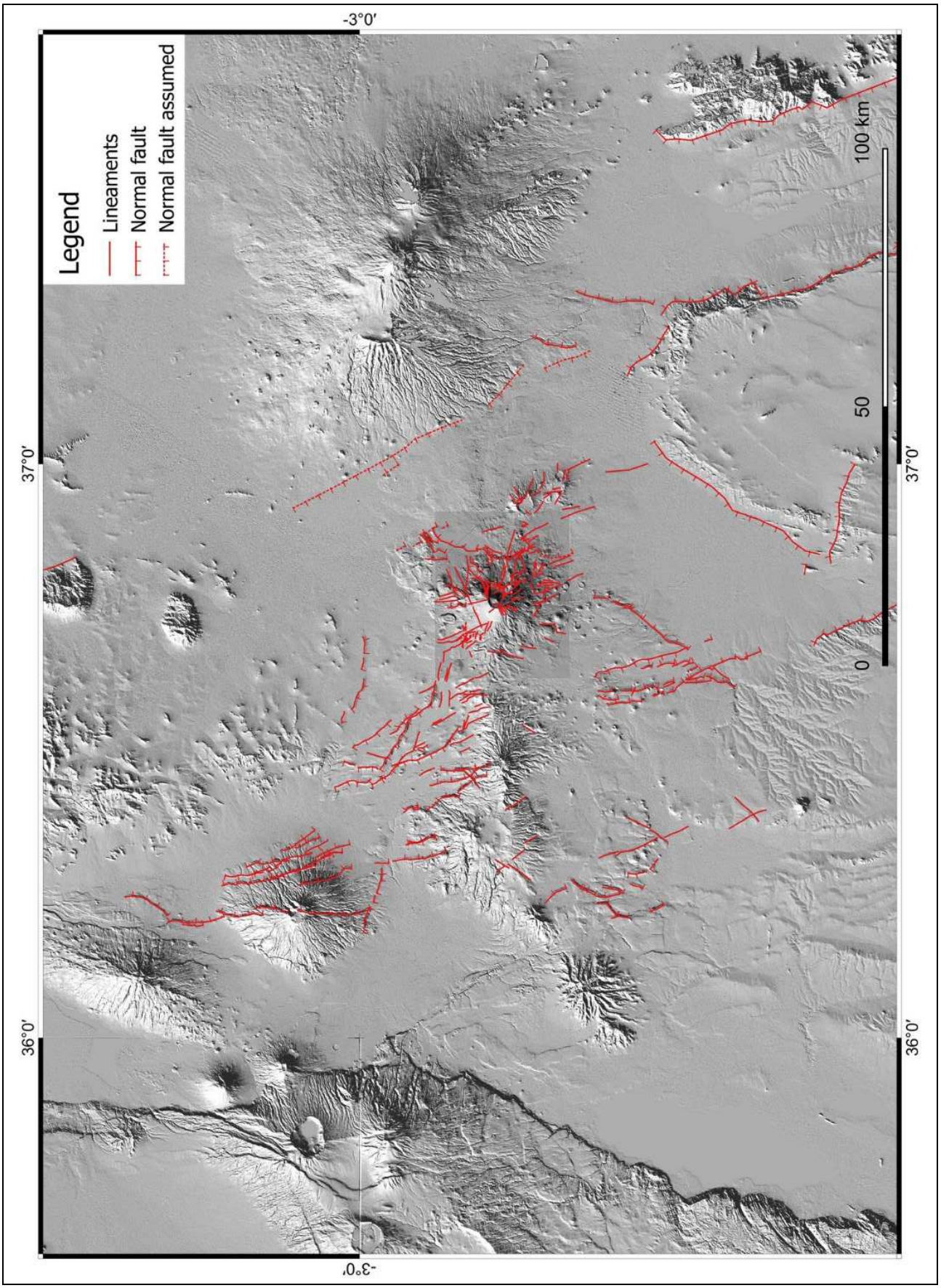

Figure 6.2: Examples for lineaments and normal faults (assumed normal faults, to be explained later below) in the major area of Mount Meru. Shaded relief SRTM DEM mosaic.

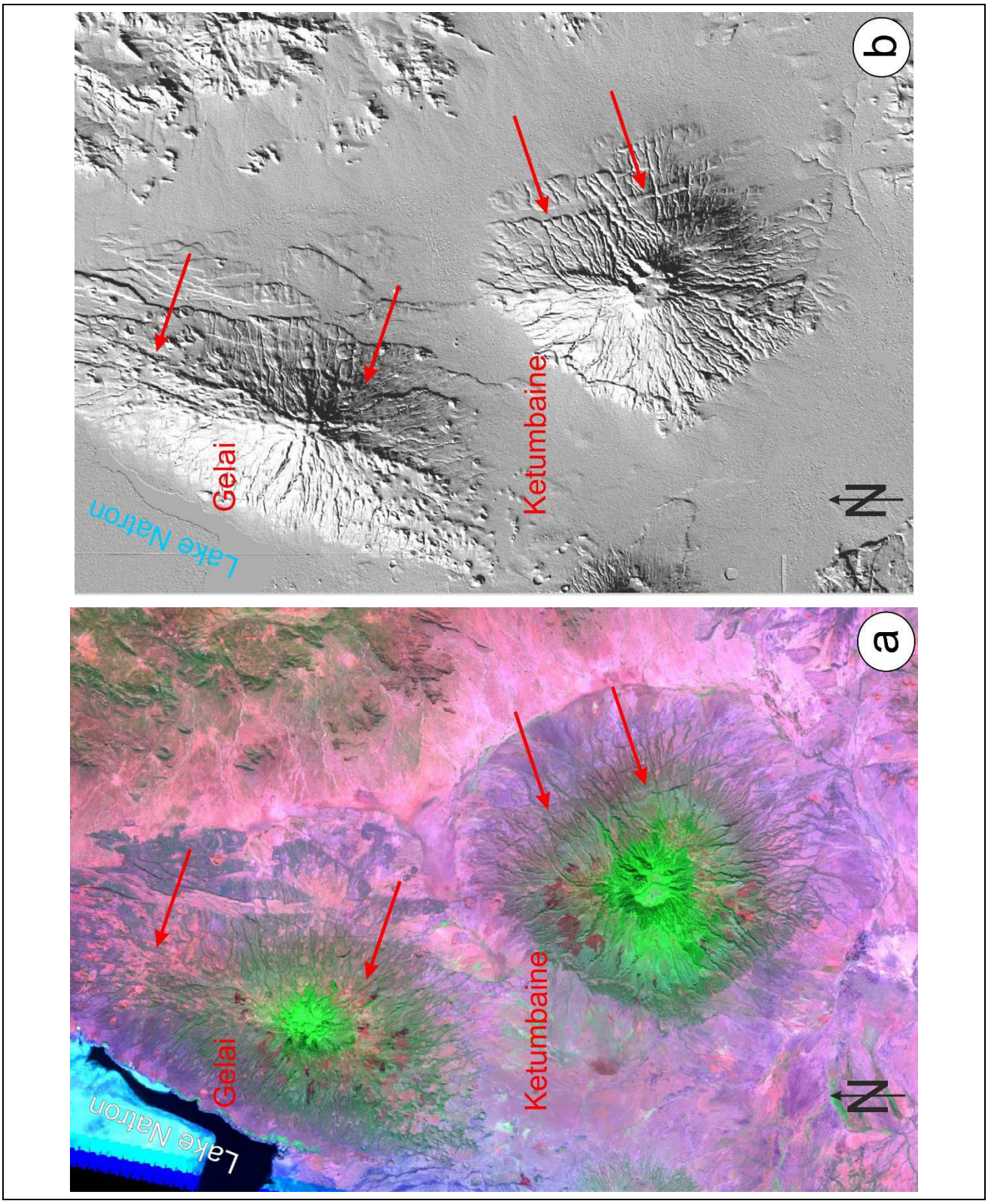

Figure 6.3: The shield volcanoes Gelai and Ketumbaine are offset by normal faulting (red arrows showing examples), which turns from a NE- at Gelai to a NW direction at Ketumbaine (red arrows). This can be attributed to a change of the structural trend of the Precambrian basement (see Fig. 5.1). a: Landsat TM bands 7,4,1 (RGB) supply spectral information about the surface´s character: “false colours” e.g. cyan: salt crust of Lake Natron, black: clear water, pink: bare rock/soil. green: vegetation. b: shaded relief 30m SRTM DEM enhances structures like faults (red arrows, examples).

Some lineaments form X-shaped conjugated faults, displaying the regional stress field and the present opening direction of the Natron-Manyara-Rift. This direction most likely displays the recent dominant rifting (Fig. 6.4).

Lineament mapping was focused to the core Mt. Meru area and to a certain extent to the surrounding area outside Mt. Meru to examine and exemplify fault- and lineament directions in a larger framework. All directions of the dominant rifts appear also inside the relatively small working area (Figures 6.5 to 6.7). The orientations of the *assumed* normal faults are not considered in the rose diagrams. Lineament lengths do not weight the rose diagrams.

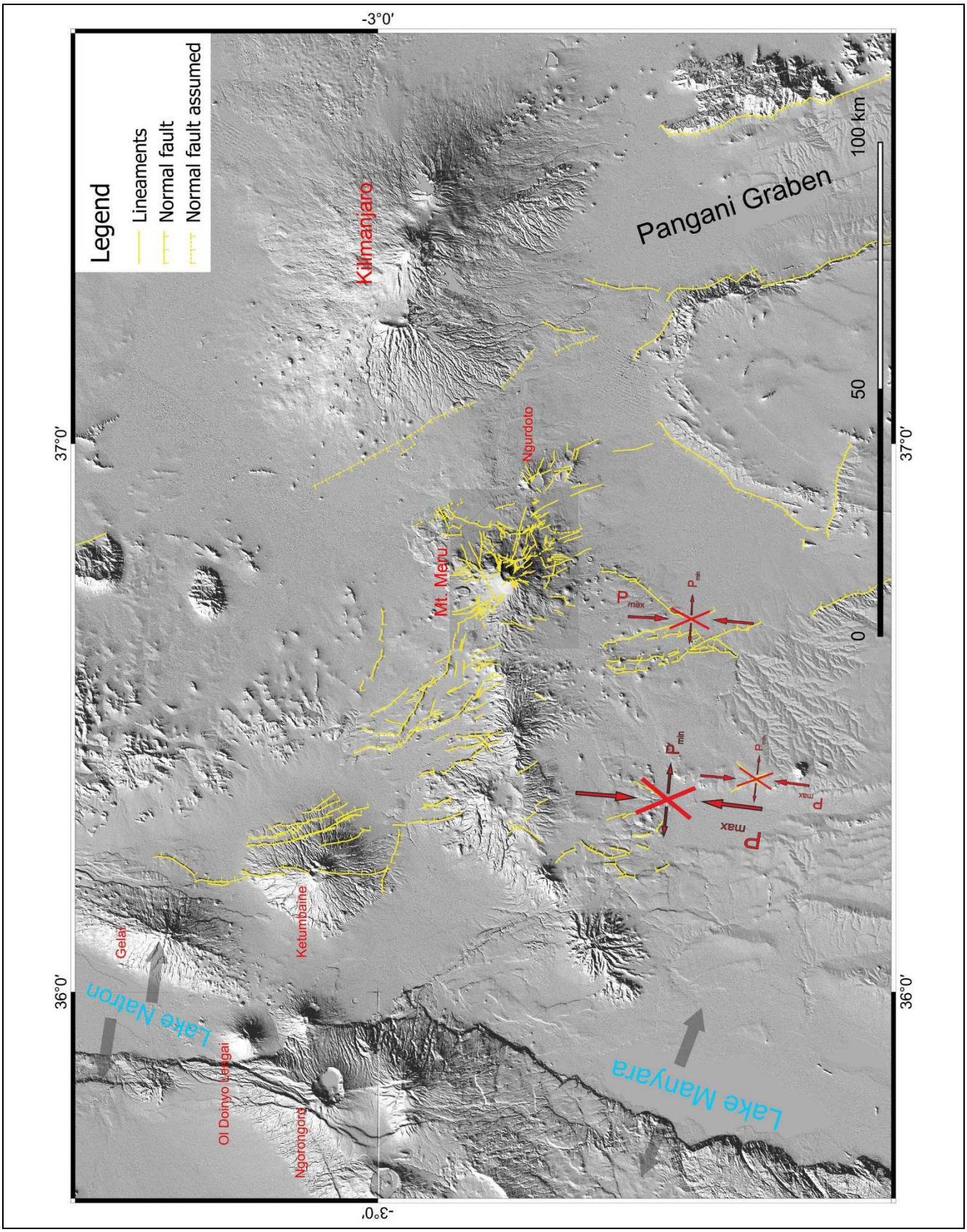

Figure 6.4: The directions of maximum principal stress can be derived from satellite imagery, regarding the X-shaped stress indicators (red lines). The acute angle between conjugated faults (red lines, three examples of more existing) is bisected by the maximum principal stress direction (P_{max}). The direction of effective minimal principal stress direction (P_{min}) corresponds in this example approximately to the opening direction of the Natron-Manyara-Rift (grey arrows).

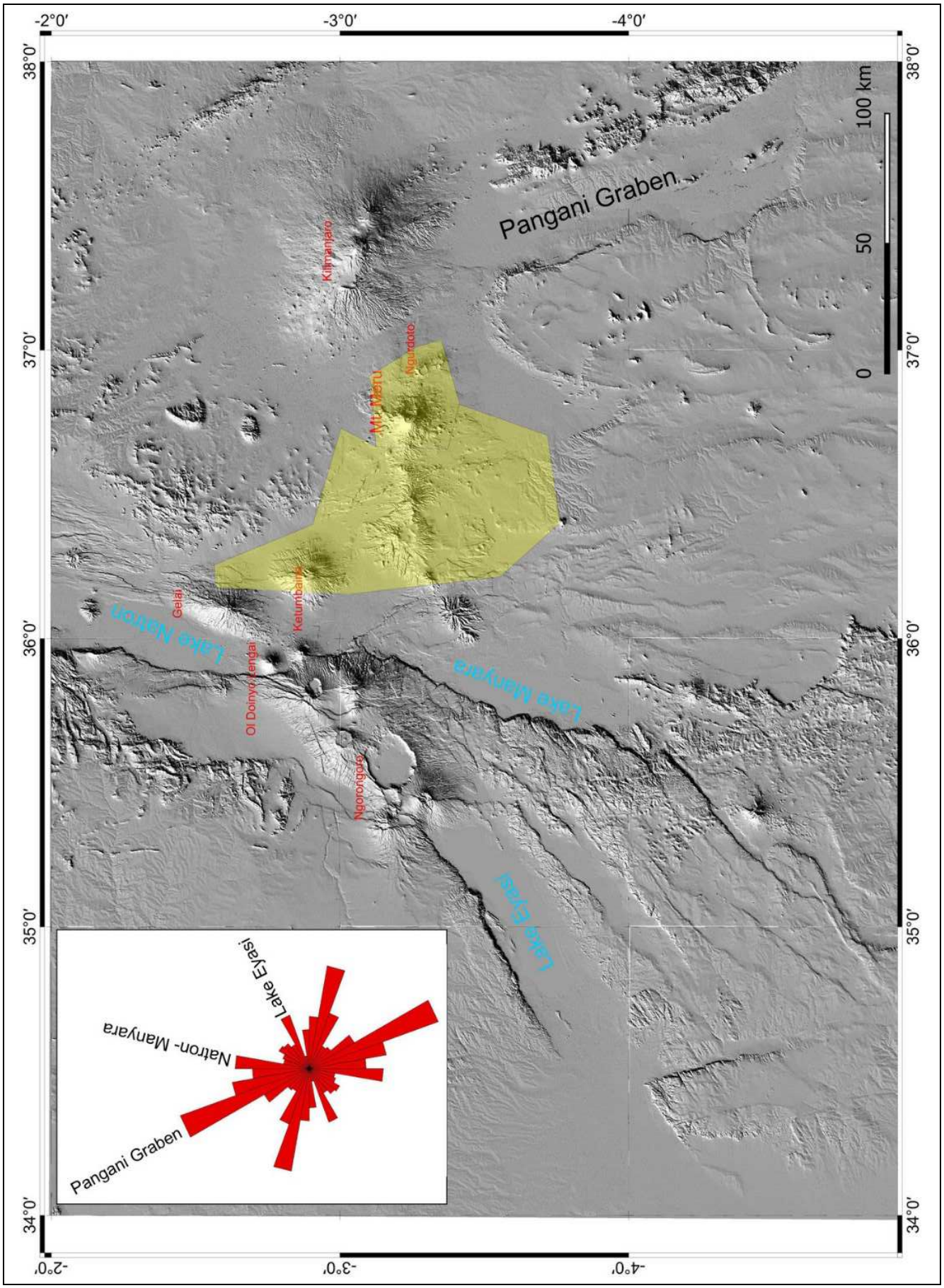

Figure 6.5: The orientations of the dominant regional rifts (Pangani Graben, Natron-Manyara and Lake Eyasi) are reflected in the extended working area (yellow polygon).

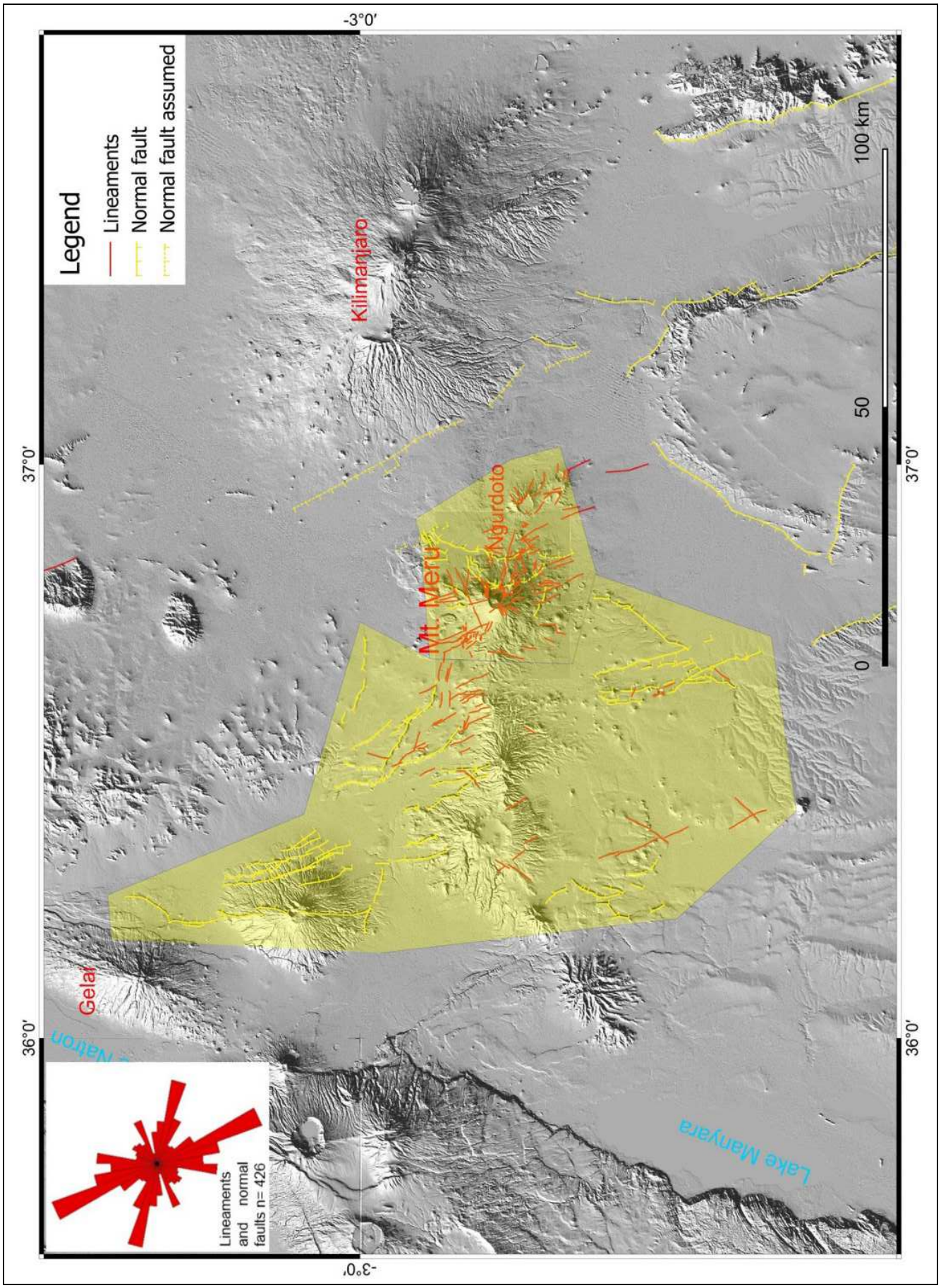

Figure 6.6: Lineaments and normal faults with rose diagram of the extended working area (yellow polygon).

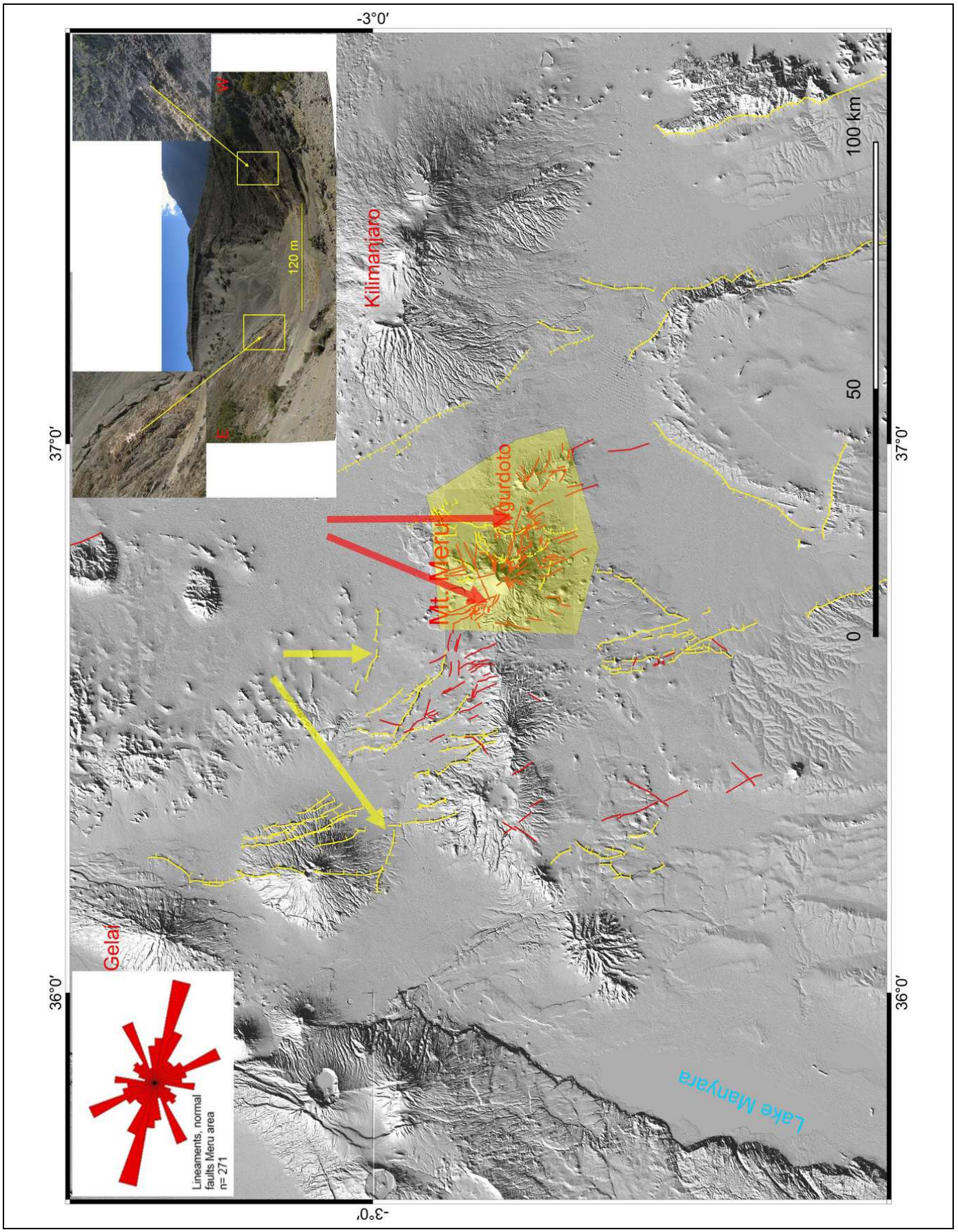

Figure 6.7: Lineaments and normal faults with rose diagram of the “core area” of Mt. Meru (yellow polygon). WNW-ESE orientations dominate this area. The inset shows hydrothermal alterations in the central ash cone corresponding to this direction.

The Mt. Meru volcano complex area is affected by all orientations of re-activated faults, which can also be found in the surrounding area. WNW-ESE orientations are dominant. This orientation shows hydrothermal alteration in the central ash cone (Fig. 6.7, see also larger field photo in Fig. 5.6).

East of Mt. Meru two major bended normal faults occur (Figures 6.8 and 6.9). The western one might have triggered the Ngare Nanyuki/Ongadongishu Lahars (reinterpreted as debris avalanches). It forms a steep step at the eastern crater rim and is partially covered by a small part of a later debris flow, which is attributed to the Momella Lahar (Fig. 6.8, dark brown colour, reinterpreted as debris avalanche by DELCAMP ET. AL., 2016).

The eastern normal fault might have triggered the Momella Lahar (reinterpreted as debris avalanche), as it widely offsets the older debris avalanche and seems to affect the Momella Lahar (reinterpreted as debris avalanches) only to a minor extent (Figures 6.8 and 6.9).

The discontinuous bending of the fault traces shows rift orientations of the active Natron-Manyara-, Eyasi- and Pangani-Rifts.

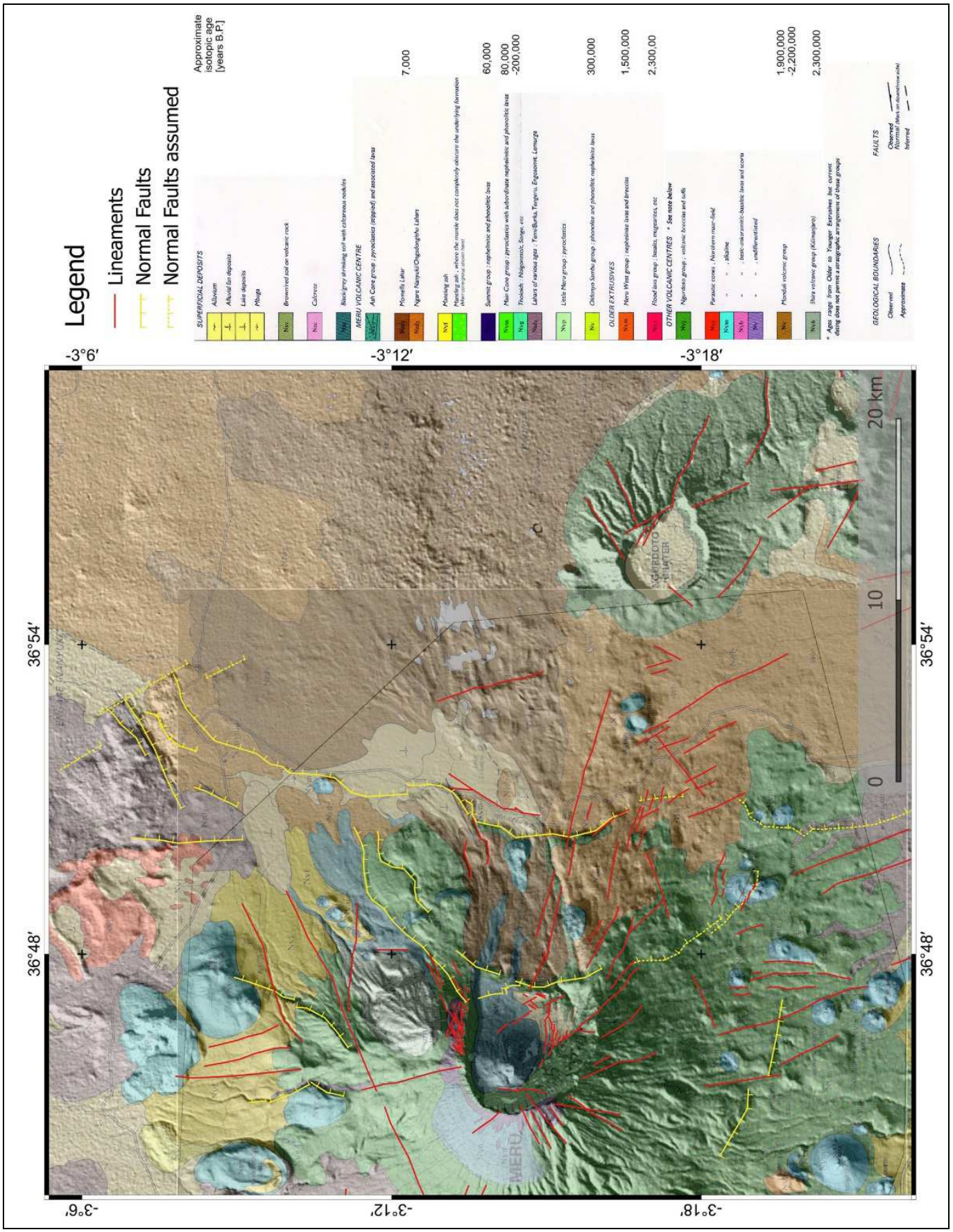

Figure 6.8: Two major bended normal faults east of Mt. Meru, which possibly have triggered the debris avalanches. Geological map (WILKINSON, P. ET AL., 1983) over shaded relief DEMs.

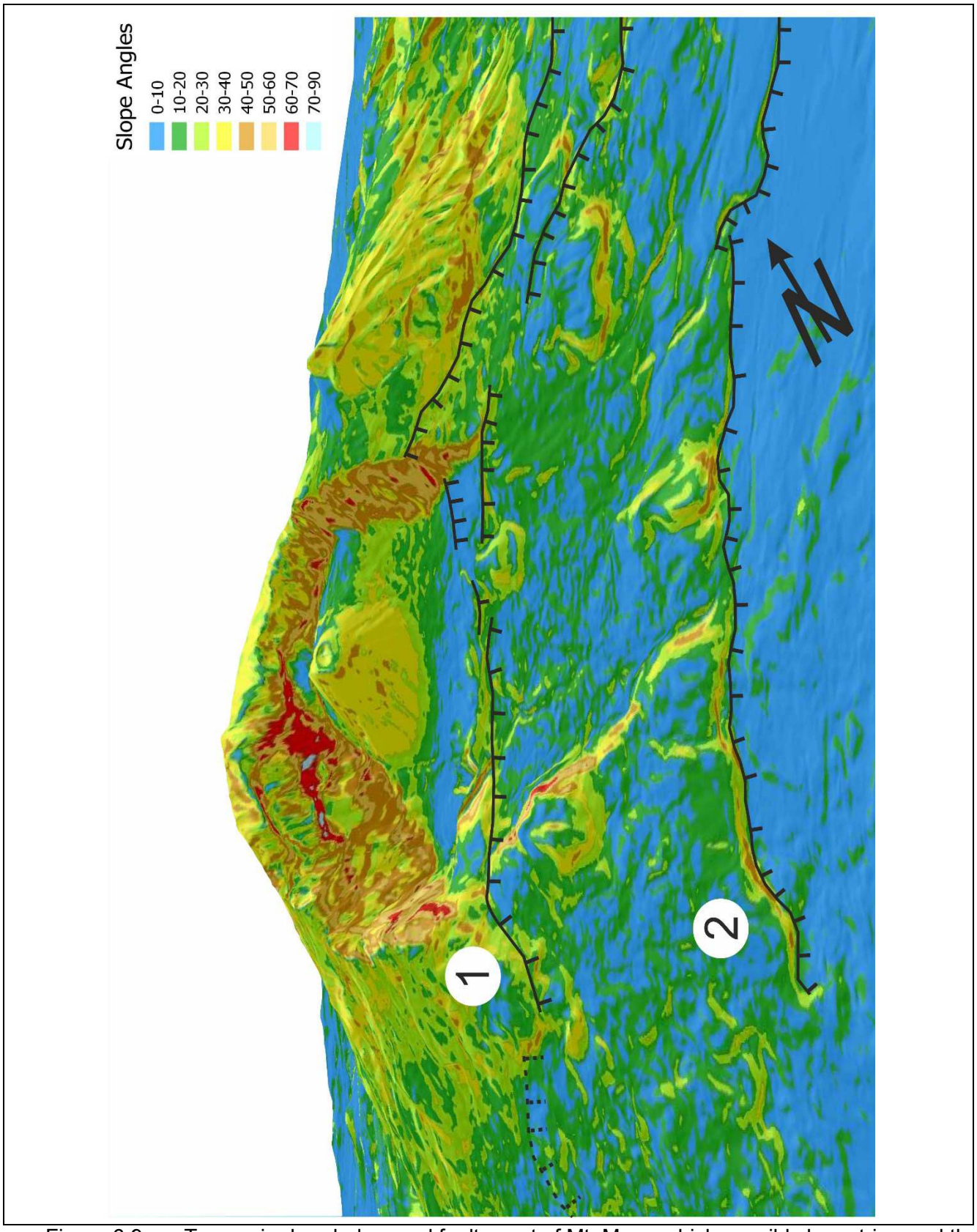

Figure 6.9: Two major bended normal faults east of Mt. Meru, which possibly have triggered the 1) Ngare Nanyuki/Ongadongishu Lahar (reinterpreted as debris avalanche) and led to the collapse of the eastern flank and 2) the Momella Lahar (reinterpreted as debris avalanches). Slope angle map derived from TSX WorldDEM projected over TSX DTM shaded relief. Perspective view into the crater with central ash cone to the west. 1.5 X vertical exaggeration.

6.2 Graben Structures

Many graben structures in the surrounding area of Mt. Meru have NW-SE orientations like the dominant Pangani Graben. Some have flanks with chains of aligned volcanoes like the Oljoro Graben (Fig. 6.10). Aligned volcanoes reflect faults of the deeper basement also in other places (Fig. 6.12).

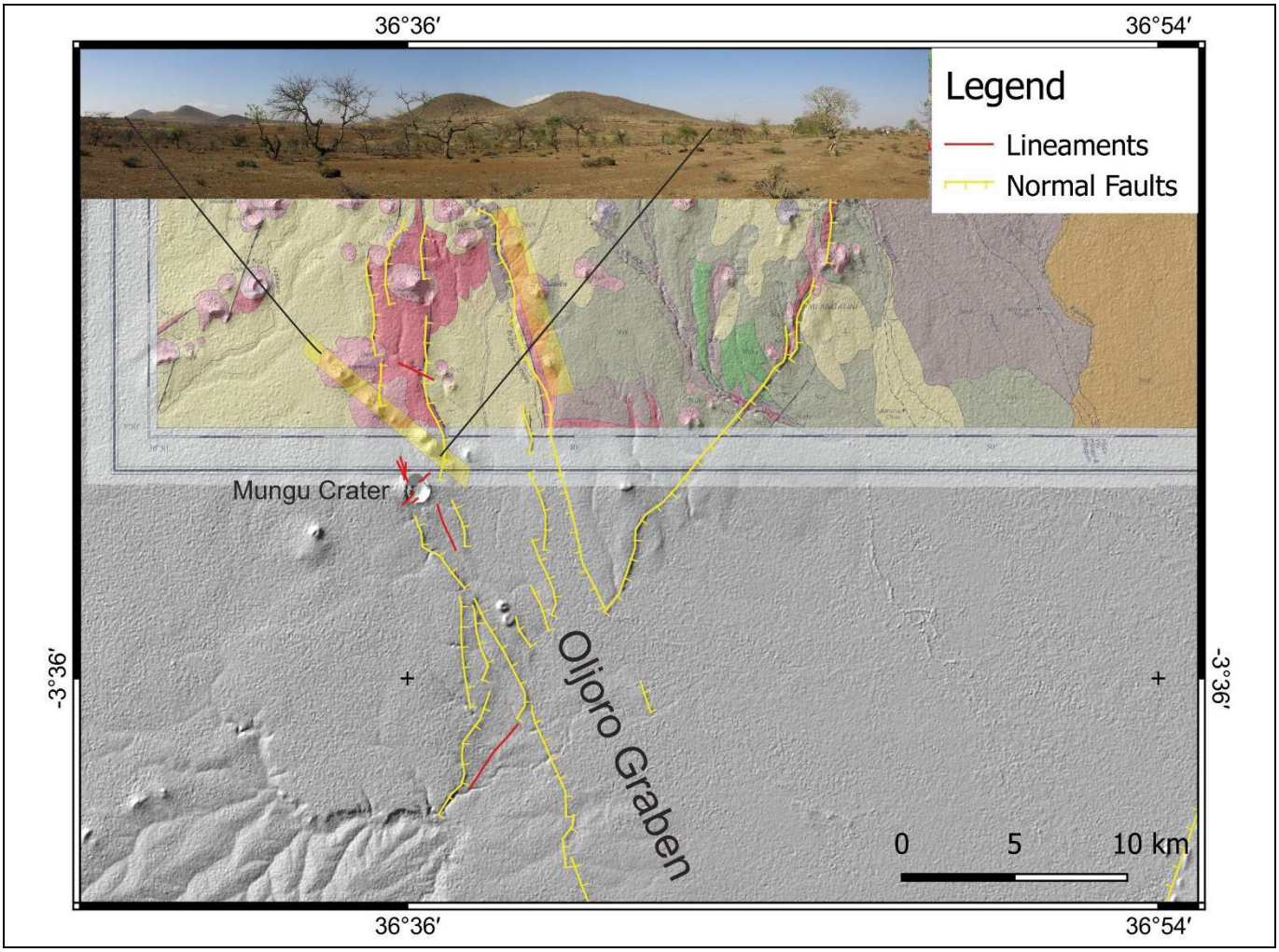

Figure 6.10: The NW-oriented Oljoro Graben with volcano-chains running parallel and NW-angular towards the flanks (transparent yellow stripes). The photo shows the angular volcanic chain as seen from Mungu Crater. Subset of the geological map (WILKINSON, P. ET AL., 1983) over shaded relief DEM.

There are structural hints, which strongly support the existence of a NW-SE orientated graben structure between Mt. Meru and Kilimanjaro (inferred “Meru Kilimanjaro Graben”). The shaded relief DEM clearly shows a (debris avalanche-filled) depression with linear borders. The western flank is covered with the major “volcanic-chain” of Ngurdoto crater and others (Fig. 6.11), the eastern flank at the foot of Mt. Kilimanjaro shows only minor aligned cones, which cut the inferred fault in similar NW-angles as at the western flank of the Oljoro Graben (Fig. 6.10, transparent yellow stripes). At the southern end of the assumed normal fault is an occurrence of hot springs (Fig. 6.11a, red dot).

The inferred “Meru Kilimanjaro Graben” would represent the “Mt. Kilimanjaro-deflected” prolongation of the Pangani Graben. The structure possibly runs even farther to NE, supported by an eastward tilted block north of the town of Namanga/Kenya (Fig. 6.12). LE GALL ET. AL. (2008) attribute this block to be part of the Aswa shear zone running NW from the eastern shoulder of the Pangani Graben through Mt. Kilimanjaro.

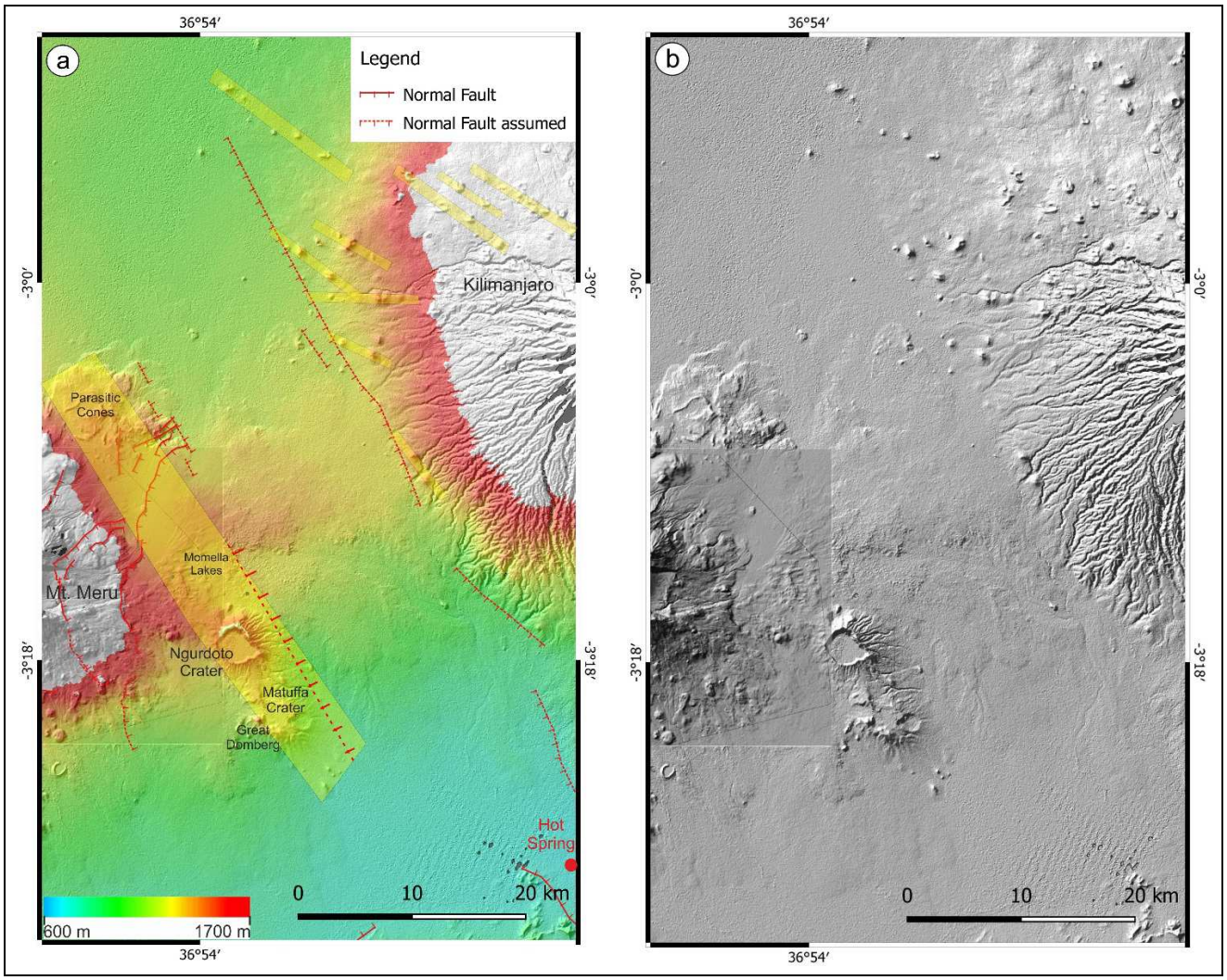

Figure 6.11: a: The NW-oriented graben structure between Mt. Meru and Kilimanjaro with normal faults, assumed normal faults and volcanic-chains (transparent yellow stripes along the flanks. The topographic heights inside the structure represent the debris avalanches emerging from Mt. Meru. Colour coded DEM over shaded relief DEMs. b: The un-interpreted shaded relief DEMs reveal the linear graben structure between Mt. Meru and Mt. Kilimanjaro even better.

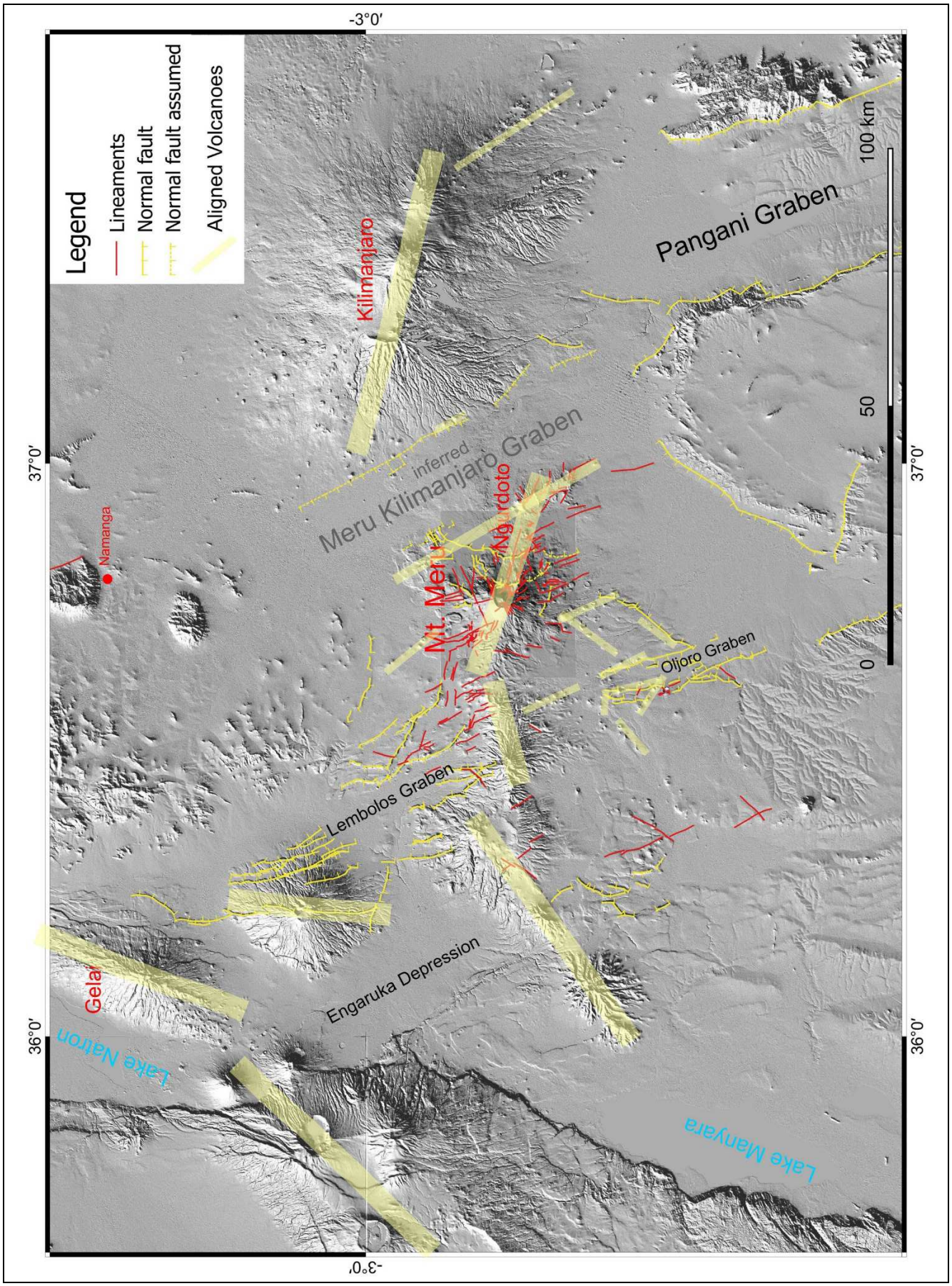

Figure 6.12: Overview of graben structures (most are NW-oriented), faults and fault-related volcanic-chains of the expanded working area over shaded relief DEMs.

7 Ground Movements

The relatively short period of Radar-measurement (2013/07/28 to 2015/04/13) as well as surface conditions like vegetated areas and soft structures is a challenge for the detection of ground movements using Radar interferometric methods.

The SBAS-algorithm (see chapter 4) however reveals good results for the further interpretation of subsidence features.

The quality of the data processing can be validated, as Lake Manyara is also covered by the used Radar-scenes, showing subsidence as well (red areas, Figure 7.1 and following figures). Subsidence at Lake Manyara however, is well known and documented by authors using different Remote Sensing and in-situ-methods (DEUS, D. ET AL., 2013).

At Mount Meru, mainly the south-eastern part is affected by subsidence of up to 136 millimetres per year. These areas occur as clusters, which form elongated zones (Figures 7.2 to 7.4). Most of these zones are not connected direct to particular mapped lineaments, however they follow the same orientations, indicated by lineaments (e.g. normal faults, graben structures, see Figures 6.12 and 7.4) and volcanic chains at other locations of the Mt. Meru surrounding area (Figures 6.12, 7.2 to 7.4).

It is most likely, that neotectonics are the main factor for the development of these linear zones of subsidence. However, it is possible, that changes of the surface hydrology contribute also to the observed ground motions to a certain degree and interfere with tectonically induced subsidence.

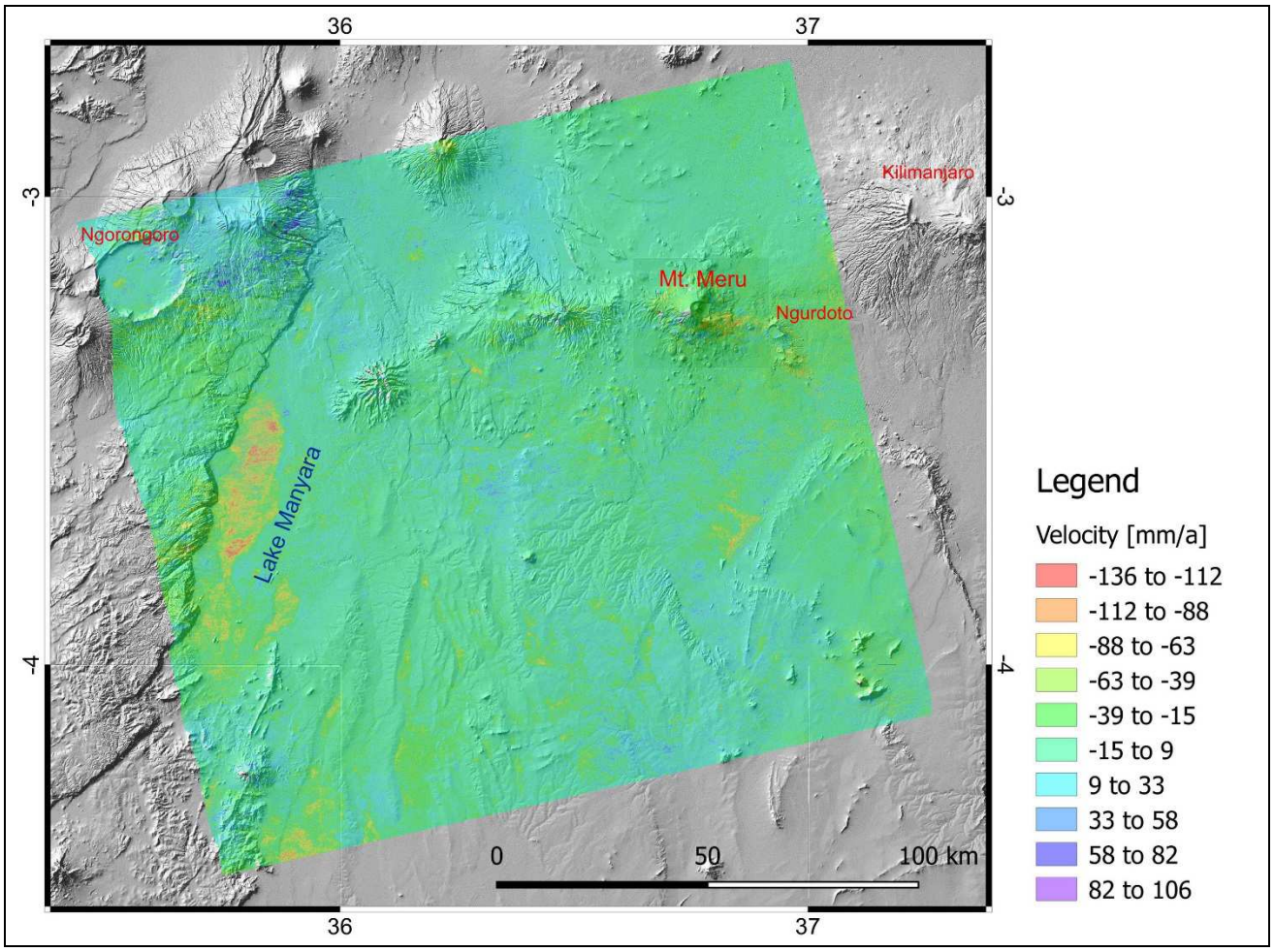

Figure 7.1: Coverage of the displacement map derived from RADARSAT-2 interferometry. Projected onto high resolution 12m TerraSAR-X WorldDEM (Mt. Meru area only) and 30m SRTM DEM shaded relief. Subsidence of Lake Manyara (red orange areas) is well documented in literature and shows similar values as subsidence at Mt. Meru.

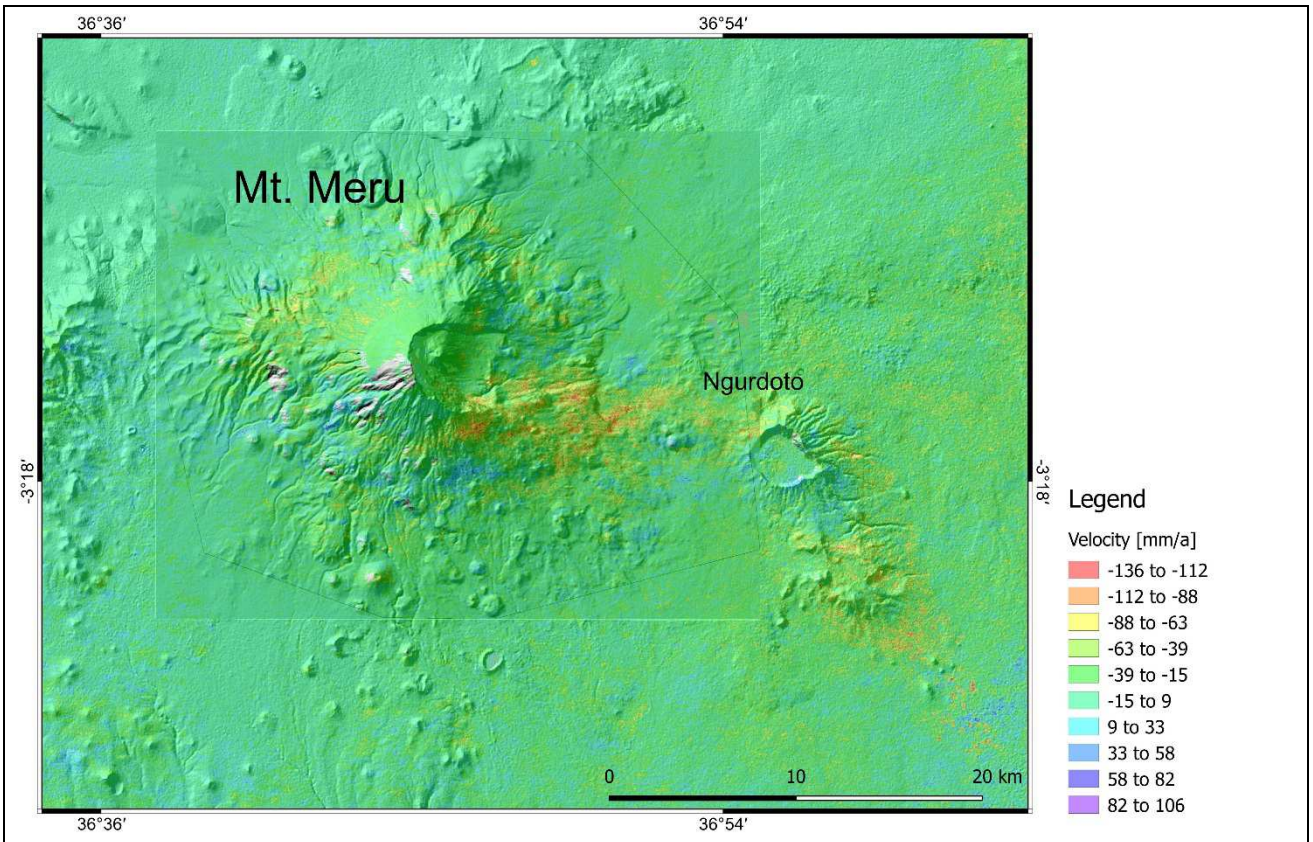
36°36′
36°54′
Mt. Meru
Ngurdoto
-3°18′
0
10
20 km
Legend
Velocity [mm/a]
-136 to -112
-112 to -88
-88 to -63
-63 to -39
-39 to -15
-15 to 9
9 to 33
33 to 58
58 to 82
82 to 106

a)

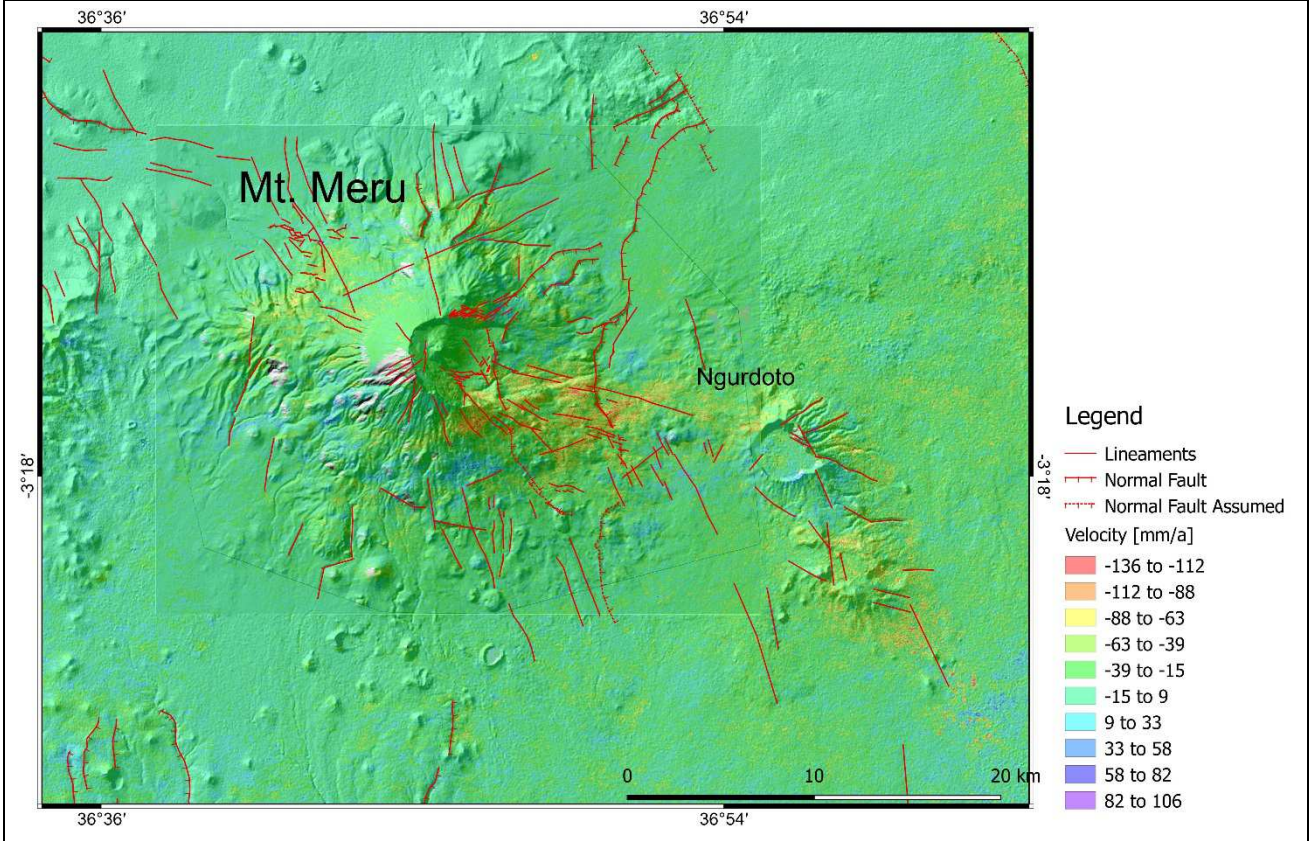
36°36′
36°54′
Mt. Meru
Ngurdoto
-3°18′
0
10
20 km
Legend
Lineaments
Normal Fault
Normal Fault Assumed
Velocity [mm/a]
-136 to -112
-112 to -88
-88 to -63
-63 to -39
-39 to -15
-15 to 9
9 to 33
33 to 58
58 to 82
82 to 106

b)

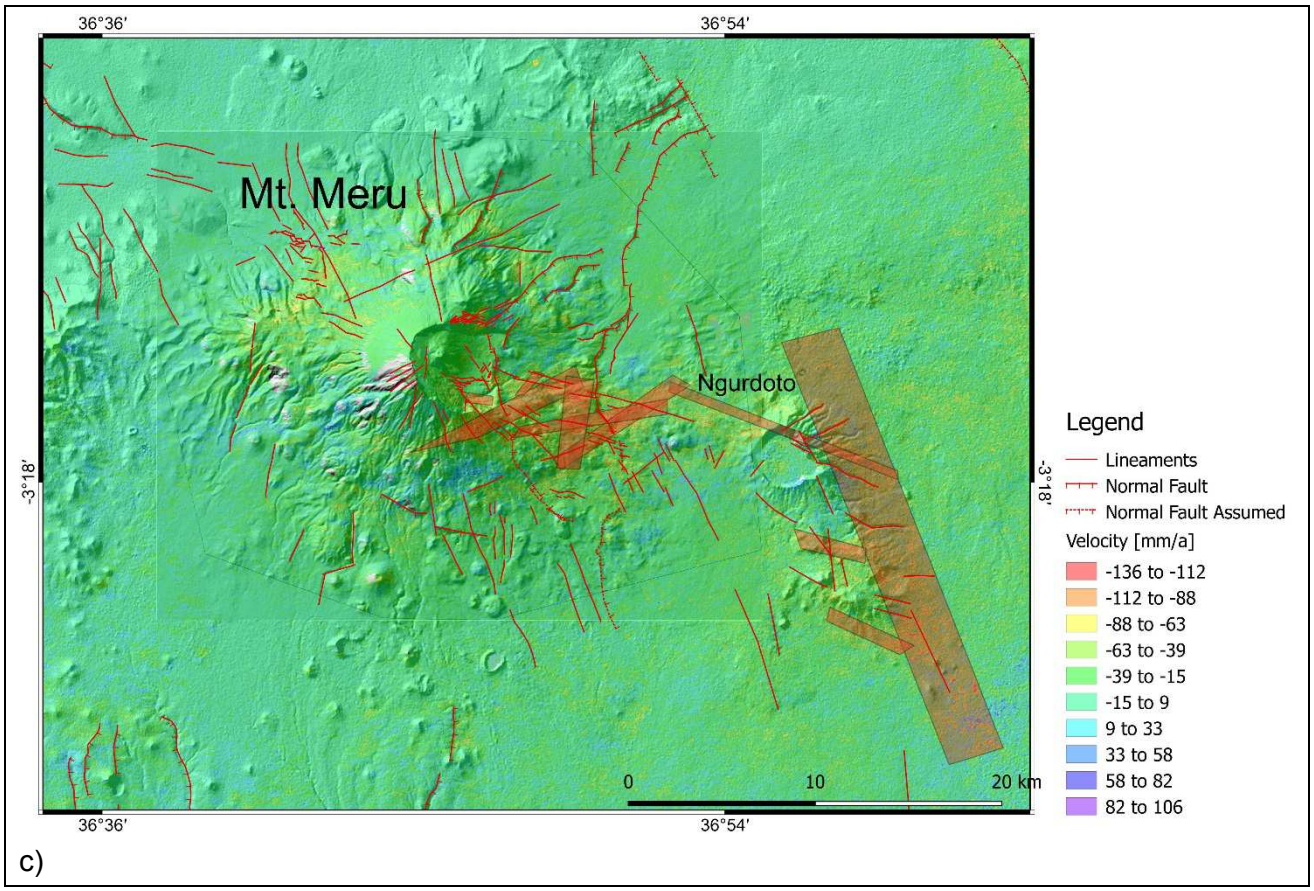

c)

Figure 7.2: Displacement maps projected onto shaded relief DEMs for better orientation. a): Clusters of subsidence. b): Clusters of subsidence and lineaments. c): Clusters of subsidence and lineaments. The transparent red stripes highlight the zones of subsidence and their orientations.

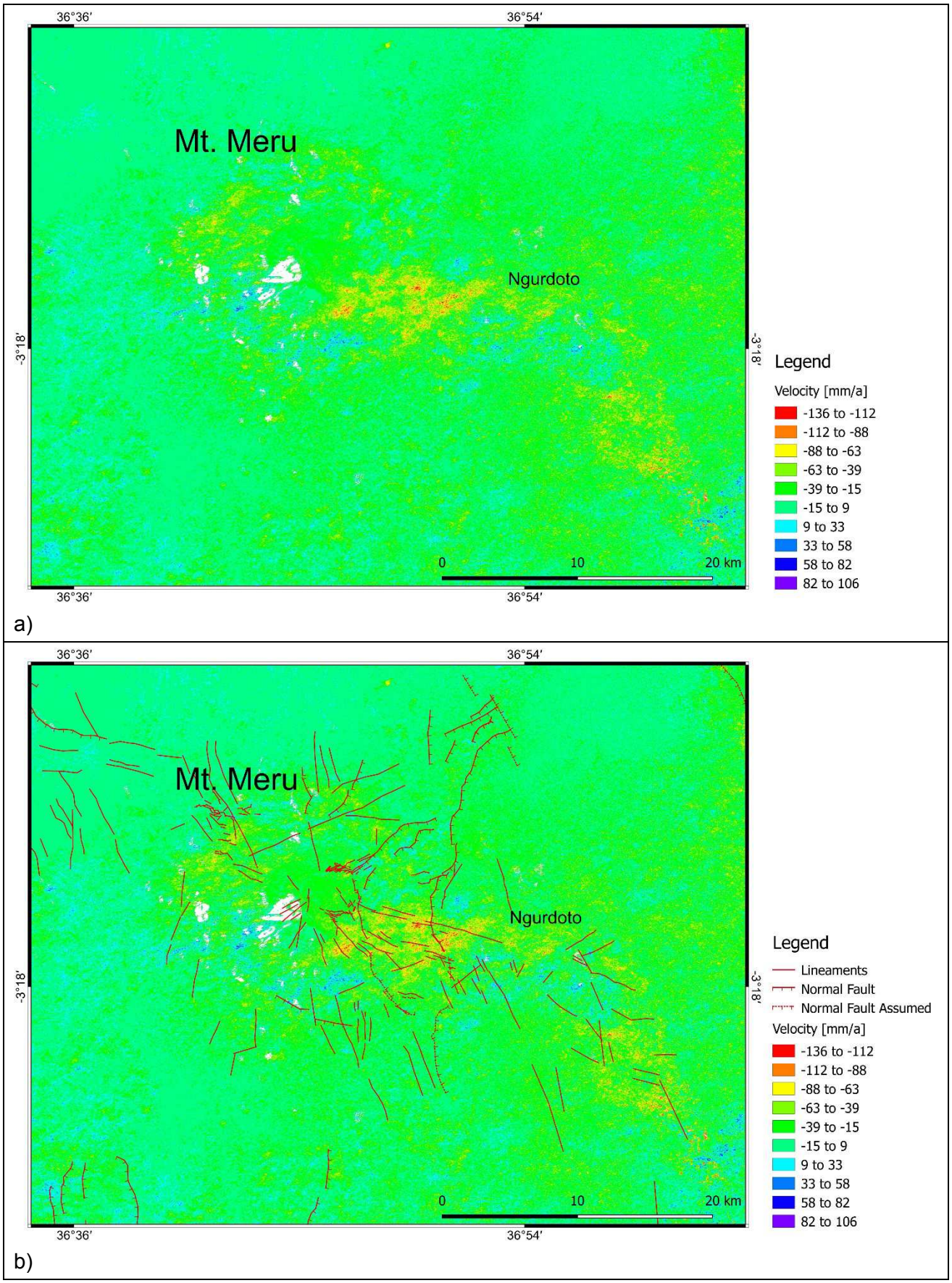
36°36′
36°54′
-3°18′
Mt. Meru
Ngurdoto
0
10
20 km
Legend
Velocity [mm/a]
-136 to -112
-112 to -88
-88 to -63
-63 to -39
-39 to -15
-15 to 9
9 to 33
33 to 58
58 to 82
82 to 106
a)
Lineaments
Normal Fault
Normal Fault Assumed
b)

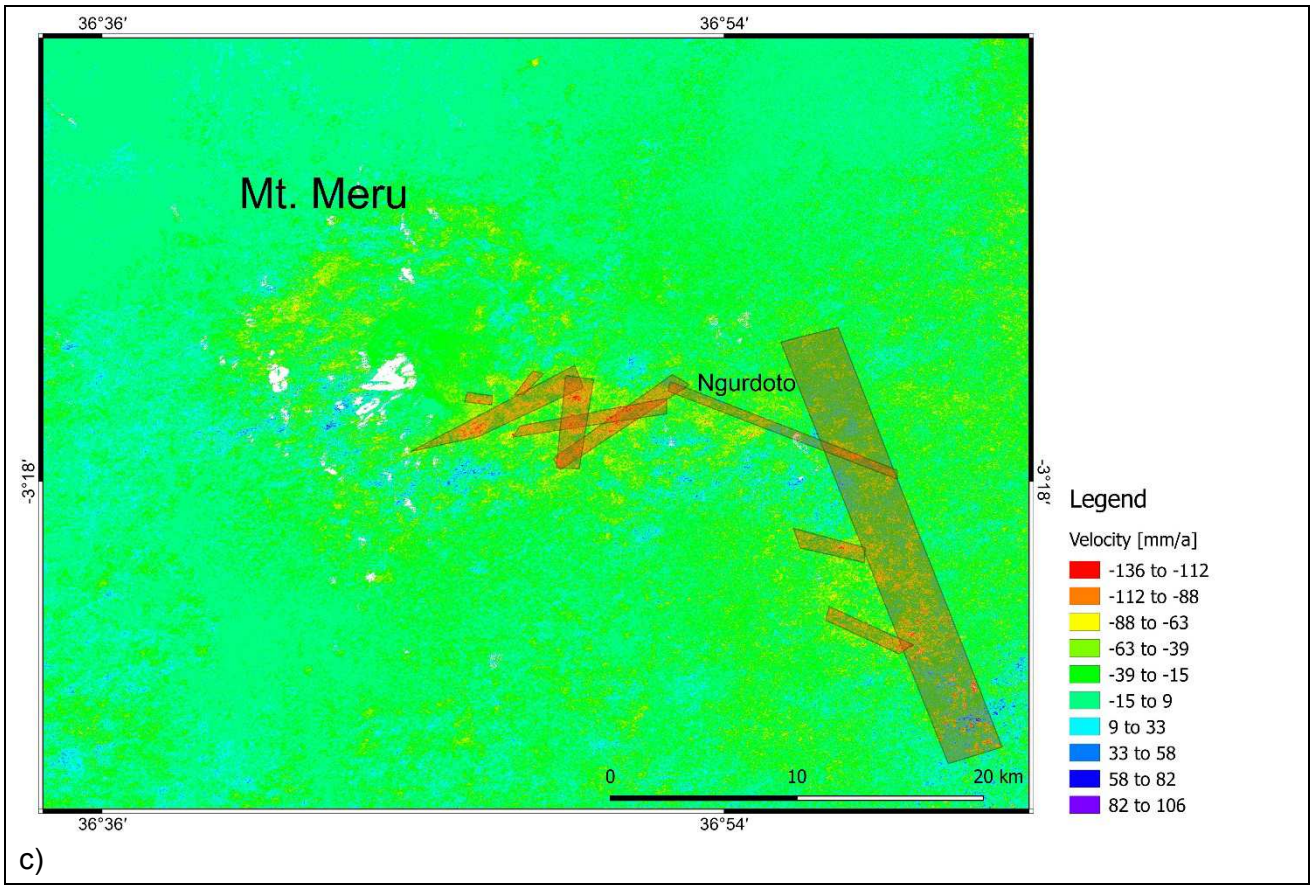

Figure 7.3: The same displacement maps as in the figures before without DEMs to enhance only zones of subsidence. White areas are unclassified due to Radar layover. a): Clusters of subsidence. b): Clusters of subsidence and lineaments. c): Clusters of subsidence and lineaments. The transparent red stripes highlight the zones of subsidence and their orientations.

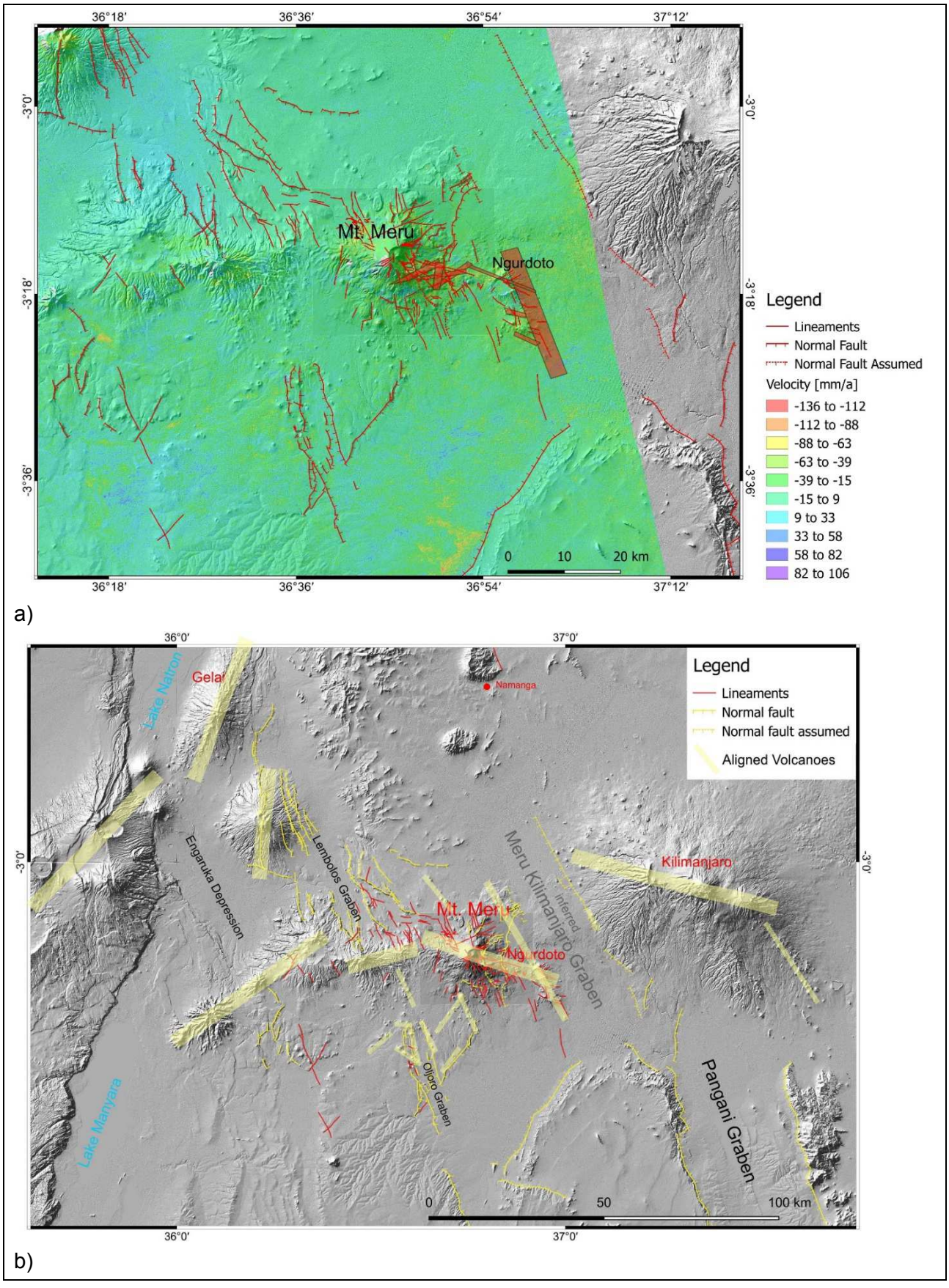

Figure 7.4: a) Displacement map projected onto shaded relief DEMs with lineaments and zones of subsidence (transparent red stripes), which display the same orientations as b) lineaments and volcanic chains of the surrounding area. See also Figure 6.12.

The zones of subsidence are mainly found in areas of moderate steepness and flat areas. Thus, subsidence seems not to be correlated to „normal slope effects“ like slope creeping. Furthermore, single zones extend over areas of different slope angles (Figure 7.5b) and different geological units (Figure 7.6).

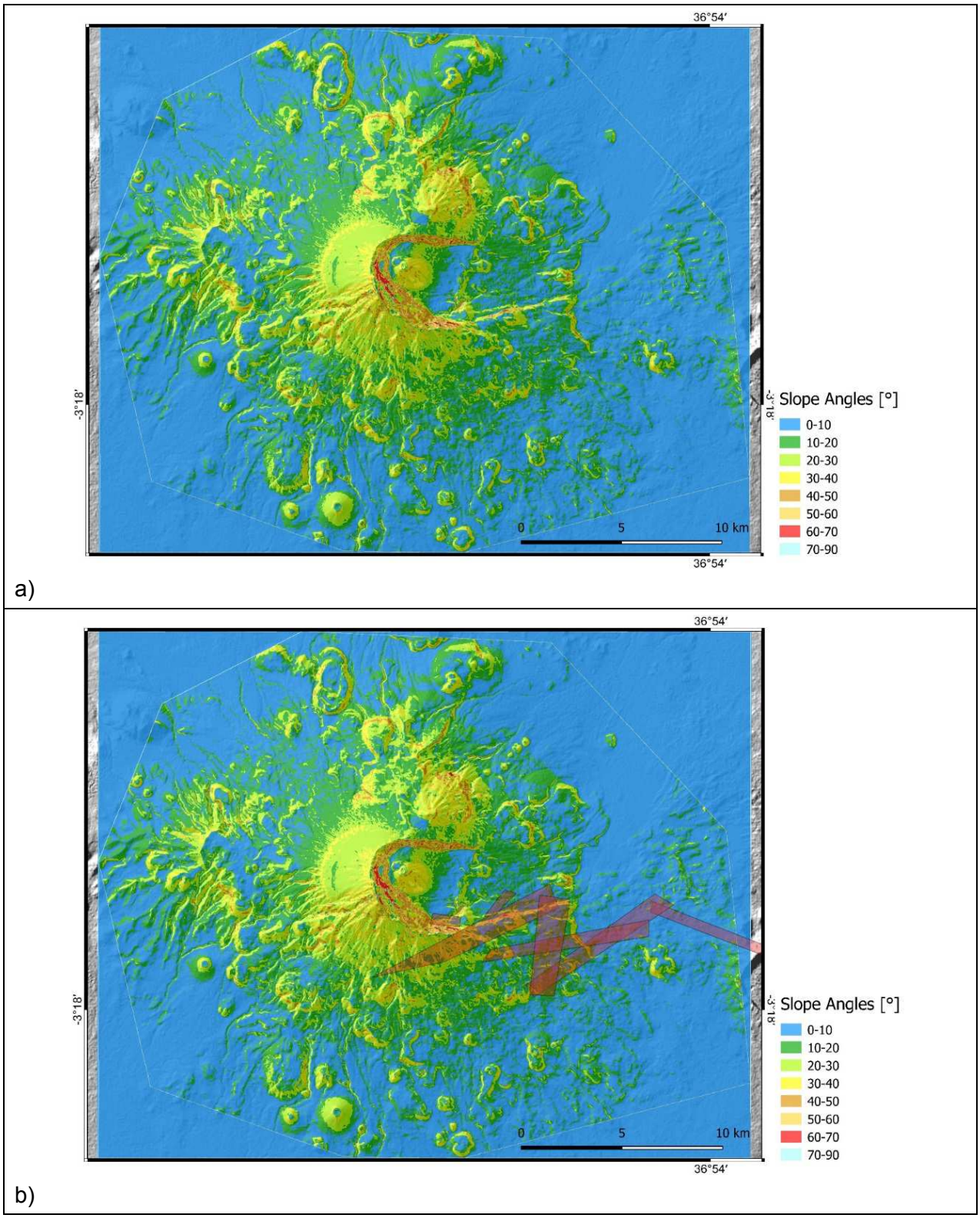

Figure 7.5: a) slope angle map derived from TSX WorldDEM. b): Subsidence zones (transparent red stripes) extend over areas of moderate- and flat slope angles.

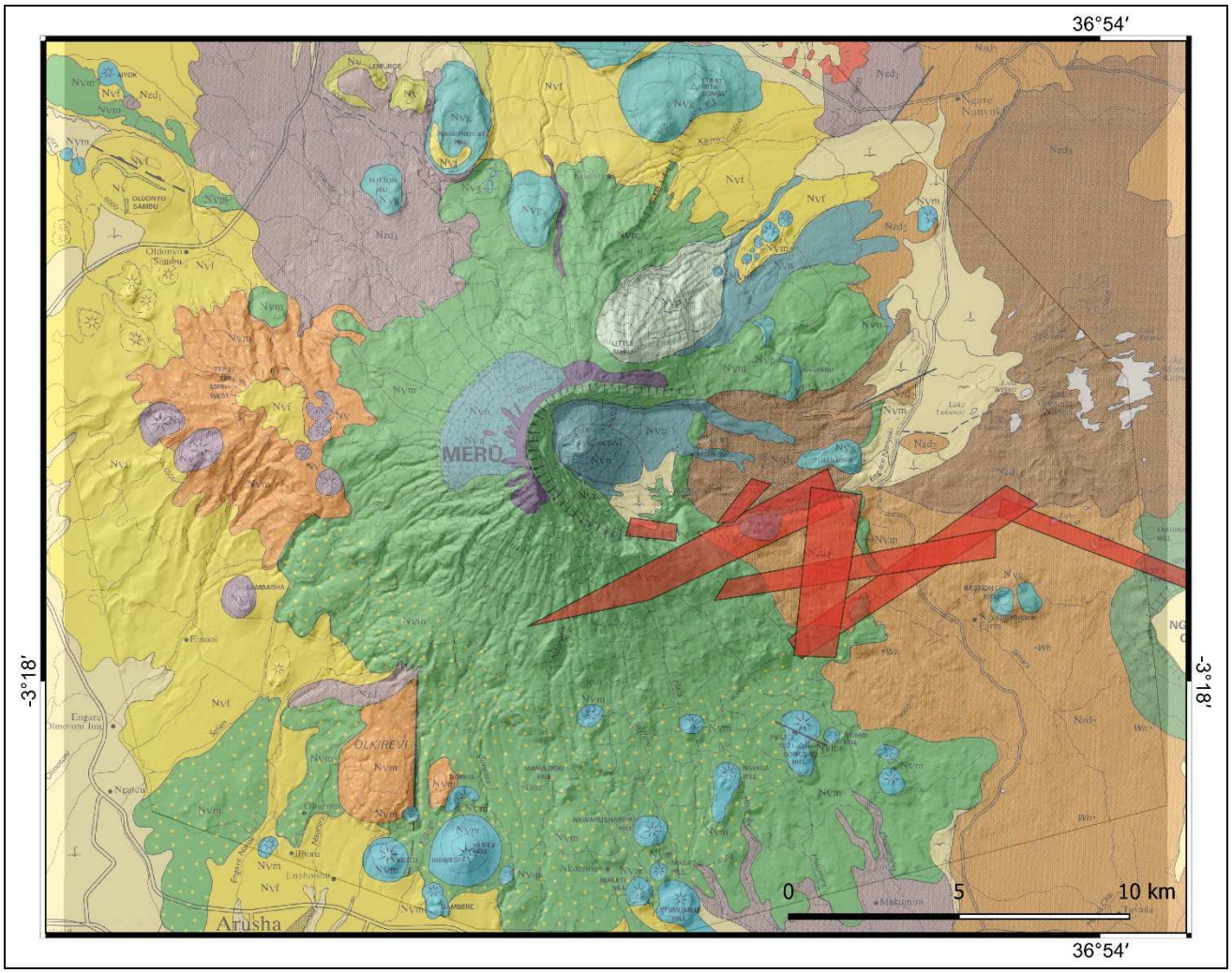

Figure 7.6: Geological map (WILKINSON, P. ET AL., 1983, legend see figure 5.3). Subsidence zones (transparent red stripes) extend over different geological units.

7.1 Suggested area for further investigations

By this time, available data, supporting geothermal exploration in a large scale is extremely limited. The area around Mt. Meru is hard to access due to steep terrain and dense vegetation cover.

The results from remote sensing, concerning structural analyses as well as ground movements, point especially towards one distinct area to be promising for further focused investigations (e.g. geophysics, Figures 7.7a and 7.7b).

In this area, lineaments of different orientations including the prominent WNW-orientation (see Figures 5.6 and 6.7) with hydrothermal alterations at the top of the central ash cone can be found intersected by zones of high subsidence, which altogether possibly are hints for increased permeability for fluids.

The topography of the land surface is relatively flat to moderate. Furthermore, access is good, as an existing road crosses the area.

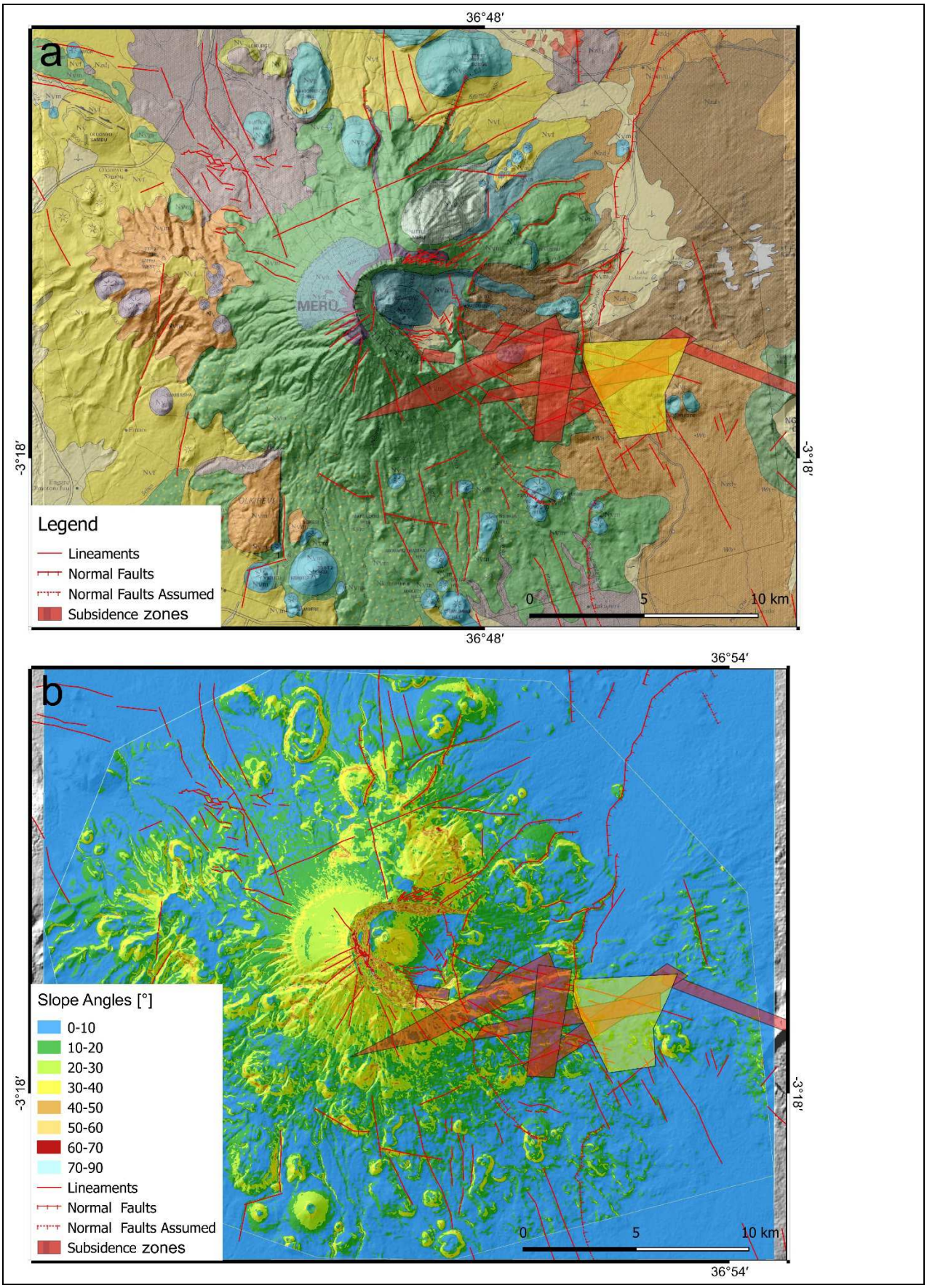

Figure 7.7: Suggested area (yellow polygon) for further investigations based on the results from remote sensing structural analyses and InSAR ground movement detection. a) Geological map over TSX-DEM. b) Slope angle map over TSX-DEM.Conclusions

8 Conclusions

Southeast of Mt. Meru an intersection of many different fault orientations can be found. Also in this area, intersecting zones of high subsidence, as detected by the InSAR study, occur. Hence, this location can be considered as highly permeable for groundwater and other fluids and represents a fitting area for further examinations.

Fault orientations east of Mt. Meru:

- WNW orientation is dominant and connected with young hydrothermal alterations in the central ash cone,
- NW orientation (Pangani Rift, Oljoro Graben, Lembolos Graben, Engaruka Depression, inferred “Mt. Meru Kilimanjaro Graben“),
- NE orientation (Eyasi Rift),
- NNE orientation (Natron-Manyara Rift).
- A “Mt. Meru Kilimanjaro Graben” can be inferred between these two mountains. It represents a possible prolongation of the “Kilimanjaro-deflected” Pangani Rift.

InSAR results:

- Elongated zones of subsidence with velocities of up to 136 mm per year.
- These zones follow the trends of existing lineaments: e.g. graben structures and aligned volcanoes.
- Zones of high subsidence in areas of moderate steepness and flat areas,
- Single zones expand over different slope angles and different geological units,
- Subsidence seems to be controlled by linear structures/ neotectonics.

Suggested area for further investigations ESE of Mt. Meru:

- Area with different lineament orientations, including WNW oriented lineaments with young hydrothermal alterations in the central ash cone,
- Intersecting zones of high subsidence,
- Flat to moderate topography,
- Good access by existing road.

9 References

BEECKMANS, B. (2014): Volcanism in Tanzania. Thesis, Atlantic International University Honolulu, Hawaii.

BERARDINO, P., FORNARO, G., LANARI, R., SANSOSTI, E. (2002): A new algorithm for surface deformation monitoring based on small baseline differential SAR interferograms. IEEE Transactions on Geoscience and Remote Sensing 40 (11), 2375–2383.

DAWSON, J.B. (2008): The Gregory rift valley and Neogene-Recent volcanoes of northern Tanzania: Geological Society of London Memoir 33, 112 p.

DELCAMP, A., DELVAUX, D., KWELWA, S., MACHEYEKI, A. AND KERVYN, M. (2016): Sector collapse events at volcanoes in the North Tanzanian divergence zone and their implications for regional tectonics. Geological Society of America Bulletin, published online on 30 June 2015 as doi:10.1130/B31119.1.

DEUS, D., GLOAGUEN, R., AND KRAUSE, P. (2013): Water Balance Modelling in a Semi-Arid Environment with Limited in situ Data Using Remote Sensing in Lake Manyara, East African Rift, Tanzania. Remote Sensing, 5, 1651-1680, doi: 10.3390/rs5041651.

FOSTER ET, A., EBINGER, C., MBEDE, E., & REX, D. (1997): Tectonic development of the northern Tanzanian sector of the East African Rift System. Journal of the Geological Society, London, Vol. 154, pp. 689–700.

LE GALL, B., NONNOTTE, P., ROLET, J., BENOIT, M., GUILLOU, H., MOUSSEAU-NONNOTTE, M., ALBARIC, J., AND DÉVERCHÈRE, J., (2008): Rift propagation at craton margin: Distribution of faulting and volcanism in the North Tanzanian divergence (East Africa) during Neogene times. Tectonophysics, v. 448, no. 1–4, p. 1–19, doi: 10 .1016/j .tecto .2007 .11 .005.

MUIRHEAD, J. D., KATTENHORN, S. A. AND LE CORVEC, N. (2015): Varying styles of magmatic strain accommodation across the East African Rift. Geochemistry, Geophysics, Geosystems, AGU Publications. 2775-2795.

QUENNELL, A. M., MCKINLEY, A.C., AND AITKEN, W.G. (1956): Summary of the Geology of Tanganyika, Part 1. Introduction and stratigraphy, Government Printer, Dar es Salaam.

RADARSAT-2, (2016): Product description, https://mdacorporation.com/docs/default-source/technical-documents/geospatial-services/52-1238_rs2_product_description.pdf?sfvrsn=10

ROBERTS, M. A. (2002): The Geochemical and Volcanological Evolution of the Mt. Meru Region, Northern Tanzania. Dissertation, University of Cambridge, United Kingdom, Christ´s College 2002.

SIEBERT, L., (1984): Large volcanic debris avalanches: Characteristics of source areas, deposits, and associated eruptions: Journal of Volcanology and Geothermal Research, v. 22, p. 163–197, doi: 10 .1016 /0377 -0273 (84)90002 -7.

ULABY, F. T., LONG, D. G. (2014): Microwave Radar and Radiometric Remote Sensing, University of Michigan Press, 984 pp.

WILKINSON, P. ET AL. (1983): Geological Map, Arusha Quarter Degree Sheet 55; Geological Survey of Tanzania.

Appendix

Waypoints of measurements and field photos as mentioned in figures. The datum of the coordinates (digital degree) is WGS84.

WP No.	X (longitude)	Y (latitude)	Altitude (m asl)	Date
1	36.8469790	-3.2378810	1623.3	18.10.2016 15:19
2	36.8286500	-3.2444810	1928.3	19.10.2016 14:58
3	36.7870400	-3.2463260	2615.1	19.10.2016 17:02
4	36.7857520	-3.2473400	2612.2	19.10.2016 17:24
5	36.7995360	-3.2292860	2495.4	20.10.2016 07:02
6	36.7864670	-3.2351490	2620.9	20.10.2016 09:13
7	36.7871110	-3.2306770	2638.9	20.10.2016 09:47
8	36.7780820	-3.2316020	2848.3	20.10.2016 11:01
9	36.7660990	-3.2291450	3355.6	20.10.2016 13:17
10	36.7634190	-3.2367580	3589.4	20.10.2016 14:37
11	36.7625870	-3.2369910	3594.9	20.10.2016 14:46
12	36.7620960	-3.2367770	3597.4	20.10.2016 15:04
13	36.7862270	-3.2427500	2571.2	21.10.2016 09:55
14	36.7856790	-3.2437010	2582.9	21.10.2016 10:02
15	36.7852510	-3.2492120	2615.1	21.10.2016 10:27
16	36.7849570	-3.2486600	2595.9	21.10.2016 10:41
17	36.7827680	-3.2509200	2578.4	21.10.2016 11:10
18	36.7894790	-3.2451900	2557.7	21.10.2016 13:18
19	36.6399640	-3.4425150	1222.2	22.10.2016 11:40
20	36.6088480	-3.5114040	1262.8	22.10.2016 12:22
21	36.6068540	-3.5204910	1235.9	22.10.2016 13:09
22	36.6069590	-3.5204840	1240.2	22.10.2016 13:23
23	36.6081160	-3.5227050	1253.9	22.10.2016 13:35
24	36.6036030	-3.5296210	1246.9	22.10.2016 14:00
25	36.6019630	-3.5287530	1209.7	22.10.2016 14:21
26	36.6012590	-3.5282940	1187.8	22.10.2016 14:32
GateMomella	36.8498200	-3.2336210	1601.4	19.10.2016 14:29
Hotspring	37.1937730	-3.4439540	853.5	23.10.2016 11:14
Hut	36.7996460	-3.2294430	2506.5	19.10.2016 18:41
Joined River	36.8056580	-3.2482190	2229.4	21.10.2016 14:47
Lake Momella	36.8915350	-3.2220840	1452.2	18.10.2016 17:08
Lake Momella, Big	36.9058870	-3.2195040	1451.0	18.10.2016 17:24
Mungu Crater	36.6058460	-3.5252720		
Swamp	36.8332670	-3.2468910	1892.9	19.10.2016 14:48
Tanapa	36.6547320	-3.3756560	1375.0	18.10.2016 11:54
View Ngurdoto	36.7917120	-3.2422540	2488.0	19.10.2016 16:14

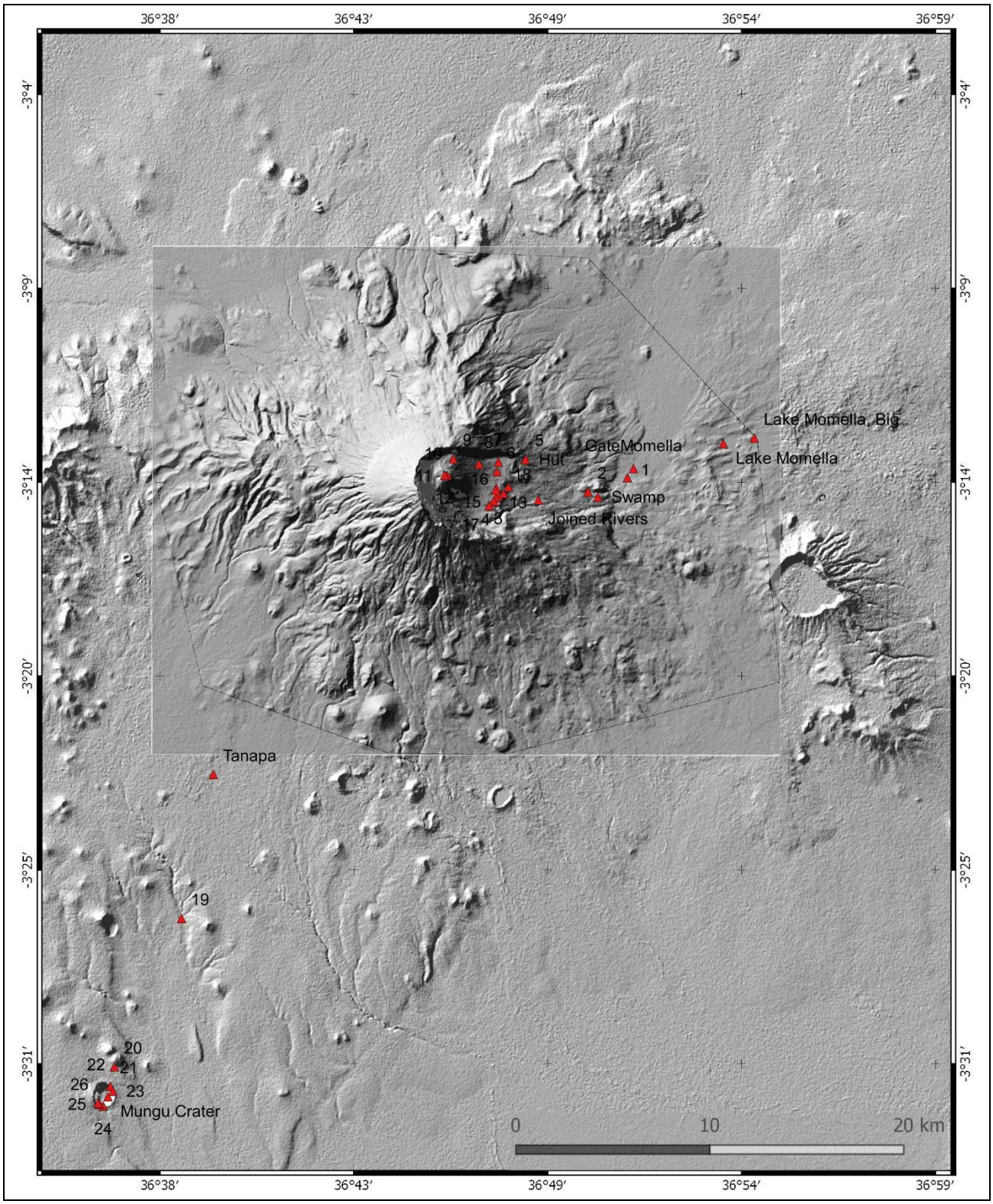

Waypoints with numbers (as referred to in figures) of the working area projected into SRTM and TSX WorldDEM elevation model.